

Review

Recent Advances, Development, and Impact of Using Phase Change Materials as Thermal Energy Storage in Different Solar Energy Systems: A Review

Farhan Lafta Rashid ^{1,*}, Mudhar A. Al-Obaidi ^{2,3}, Anmar Dulaimi ^{4,5,*}, Haitham Y. Bahlol ³
and Ala Hasan ^{6,*}

- ¹ Petroleum Engineering Department, College of Engineering, University of Karbala, Karbala 56001, Iraq
² Technical Institute of Baquba, Middle Technical University, Baquba 32001, Iraq; dr.mudhar.alaubedy@mtu.edu.iq
³ Technical Instructor Training Institute, Middle Technical University, Baghdad 10074, Iraq; haitham_yaqout@mtu.edu.iq
⁴ College of Engineering, University of Warith Al-Anbiyaa, Karbala 56001, Iraq
⁵ School of Civil Engineering and Built Environment, Liverpool John Moores University, Liverpool L3 2ET, UK
⁶ VTT Technical Research Centre of Finland Ltd., P.O. Box 1000, FI-02044 Espoo, Finland
* Correspondence: farhan.lefta@uokerbala.edu.iq (F.L.R.); a.f.dulaimi@uowa.edu.iq (A.D.); ala.hasan@vtt.fi (A.H.)

Abstract: The efficient utilization of solar energy technology is significantly enhanced by the application of energy storage, which plays an essential role. Nowadays, a wide variety of applications deal with energy storage. Due to the intermittent nature of solar radiation, phase change materials are excellent options for use in several types of solar energy systems. This overview of the relevant literature thoroughly discusses the applications of phase change materials, including solar collectors, solar stills, solar ponds, solar air heaters, and solar chimneys. Despite the complexity of their availability and high costs, phase change materials are utilized in the majority of solar energy techniques because of the considerable technical improvements they provide. While numerous studies have investigated the progress of phase change materials used in solar energy applications such as photovoltaic systems, it is vital to understand the conceptual knowledge of employing phase change materials in various types of solar thermal energy systems. Investigations into the use of phase change materials in solar applications for the purpose of storing thermal energy are still being carried out to upgrade the overall performance. This paper briefly reviews recently published studies between 2016 and 2023 that utilized phase change materials as thermal energy storage in different solar energy systems by collecting more than 74 examples from the open literature. This study focuses on demonstrating the maturity of phase change materials and their integration into solar energy applications. Based on the findings, proposals for new research projects are made.

Keywords: phase change materials (PCMs); solar energy; energy storage; solar energy technology; energy storage system



Citation: Rashid, F.L.; Al-Obaidi, M.A.; Dulaimi, A.; Bahlol, H.Y.; Hasan, A. Recent Advances, Development, and Impact of Using Phase Change Materials as Thermal Energy Storage in Different Solar Energy Systems: A Review. *Designs* **2023**, *7*, 66. <https://doi.org/10.3390/designs7030066>

Academic Editors: Surender Reddy Salkuti and Dibin Zhu

Received: 12 April 2023

Revised: 4 May 2023

Accepted: 15 May 2023

Published: 17 May 2023



Copyright: © 2023 by the authors. Licensee MDPI, Basel, Switzerland. This article is an open access article distributed under the terms and conditions of the Creative Commons Attribution (CC BY) license (<https://creativecommons.org/licenses/by/4.0/>).

1. Introduction

Even though solar energy has been used passively since prehistoric days, its technical application emerged in 2013 [1]. The development of solar thermal collector equipment from 1877 to the current times has improved human living in terms of comfort and economics [2]. Solar energy is a time-dependent renewable source of energy that is inexhaustible and eco-friendly. Among the most often used applications of solar energy is for thermal purposes. On the other hand, thermal energy storage is an efficient way to combat the sporadic and diffuse character of solar energy [3]. Techniques for energy storage can work towards closing the gap between supply and demand for energy. Among the most feasible methods for storing solar energy involves the utilization of specific organic

and inorganic substances, which are referred to as phase change materials (PCMs), which enable the latent heat of fusion to be harnessed [4]. To improve the thermal performance of solar heating systems, PCMs can be used as an effective tool. PCMs can effectively store additional thermal energy during the day through fusion and release it at sunset via solidification at a consistent temperature, which leads to a higher storage efficiency.

PCM has a number of benefits. Specifically, its high heat storage capabilities compared to other heat storage materials lead to a decrease in the size of the thermal storage facility [5]. The isothermal phase change feature of PCMs, wherein heat is charged and discharged at a virtually fixed temperature (phase change temperature) matching the phase transition, seems to be another significant benefit. As a consequence, they are perfect for applications involving space heating where thermal comfort can be attained by reducing temperature swings [6]. However, PCMs have a number of demerits such as PCM systems necessitating a long operational time to recuperate the installation cost [7]. Conventional PCMs also have other drawbacks such as low thermal stability, thermal cycling, and low thermal conductivity [8,9]. In addition, the super-cooling effect lowers the PCM's efficiency, leading to inadequate heat recovery, making it impossible to fix the PCM system without damaging it. To improve PCMs, several investigators have attempted to add various compounds; unfortunately, this has led to lower performance [10,11]. Prior to installation, the PCM's extremely poor thermal conductivity must be increased since it hinders heat transfer during the solid–liquid transition [12]. Phase segregation may happen in PCM because it may contain many elements, which would undermine its long-term stability [13]. Building envelope organic PCMs have a substantial impact on fire safety. In using organic PCMs in building envelopes, scientists have advised using fire retardants to increase fire safety [14,15].

Despite that there has been a number of attempts to review the implementation of PCMs in different solar energy systems, scholars focused on discussing the concepts of these materials with outlining the influential parameters towards its implications in the solar energy industry. For instance, Nazir et al. (2019) [16] focused on the influences of thermos-physical properties of PCMs such as the melting point, and density and thermal conductivity of the organic, and inorganic materials on their implication in thermal energy storage applications. Additionally, Sikiru et al. (2022) [17] carried out a comprehensive review that provided a thorough examination of the recent advances and impact of PCMs on solar energy systems. Specifically, the authors described how photovoltaic (PV) systems could be improved in terms of performance by integrating heat storage devices into the PV cell energy harvesting. Additionally, it covered the techniques for configuring thermal storage, evaluation of PCM type and hybrid performance, PCM entry requirements, and property testing, as well as advancements in heat and mass transfer fluids for solar energy harvesting and thermal storage mechanisms and their uses. However, both Nazir et al. (2019) [16] and Sikiru et al. (2022) [17] have not covered the potential applications of PCMs in other solar energy fields such as solar air heater, a solar pond, solar collector, solar still, and a solar chimney.

This study discusses the applications of PCMs in solar collectors, solar still, solar ponds, solar air heaters, and solar chimneys. Thoroughly, a variety of technical, research, and development approaches pertaining to PCMs are addressed. Additionally, a full grasp of the characteristics of PCM is outlined to be improved and utilized in a range of applications. The findings of the current investigation may guide future research since they will help scientists understand the numerous advancements made in PCM, which still require further advancement.

2. PCMs in Different Solar Energy Systems

The use of PCMs in solar thermal facilities is meant to boost the intensity of the heat that is stored as a result of the conversion of solar energy. The system elements in which PCMs are deployed are frequently identified in the literature to be traditional thermal energy storage devices, for example water tanks [18–20] or systems with a separate tank filled just with PCM [21]. The next sections illustrate the evaluation of the conducted

studies on the utilization of PCMs in solar collector systems, solar stills systems, solar bond systems, solar air heater systems, and solar chimney systems. Several aspects will be discussed for each solar energy system including the configuration, studied parameters and highlighting of the most interesting results.

2.1. Solar-Collector-Related Studies

A solar collector system is a technology that harnesses solar power to produce heat or electricity using sun radiation. There are two main types of solar collectors: photovoltaic (PV) (to generate electricity) and thermal (to heat water or air) collectors. A flat plate or a set of tubes that absorb sunlight and transmit the heat to a fluid or air that is pumped through the system make up the fundamental structure of a thermal solar collector [22]. The amount of sunlight available, the angle and orientation of the collector, the type of fluid utilized, and the temperature of the air or water heated, and the system's insulation all have an impact on how well a solar collector performs. By choosing the right collector design and size, maximizing the orientation and tilt of the collectors to maximize solar radiation, using premium building materials, and limiting heat losses through adequate insulation, enhancing the effectiveness of a solar collector system is attainable [23]. To guarantee optimum efficiency and the system's longevity, proper system maintenance, including routine collector cleaning of the panels to remove dust or debris is essential [24]. Solar collector systems can offer a clean and sustainable energy source for a number of uses, including electricity generation, hot water production, and residential and commercial heating, with proper design and implementation. Overall, solar collectors can decrease carbon emissions and energy expenses while also raising a property's value.

This section discusses the recent studies that focused on the utilization of PCMs as thermal energy storage in solar collectors while highlighting the benefits of PCMs, which undoubtedly have influenced their analysis and conclusions.

A relatively new proposal for an evacuated tube collector/storage (ETC/S) system including a PCM was proposed in 2016 by Feliński and Sekret [25]. Experiments were carried out to investigate the impact of incorporating commercial-grade paraffin as a PCM in evacuated tubes with heat pipes, with the aim of enhancing the thermal performance of ETC/S systems. The melting temperatures of the hydrocarbons that make up paraffin wax typically range from 47 to 68 °C. The precise melting point of paraffin wax might change depending on the unique makeup of the paraffin wax. Furthermore, the total amount of useable heat as a function of the presence of PCM in ETC/s. By allowing the recovery of heat that had been stored throughout the discharge cycle, the employment of paraffin has augmented the solar thermal operational time. Clearly, it was possible to raise the heating temperature of the medium to a practical level (approximately 45 °C). The findings also demonstrated that the paraffin-combined ETC/S system produced a total amount of useable heat that raised by 45–79% if compared to an ETC (Figure 1). These findings were reported throughout the discharge cycle considering the mass flow rate of the heating fluid.

In 2016, a numerical analysis carried out using an Artificial Neural Networks model was provided by Serale et al. [26]. These simulations were carried out to evaluate the code and get a rough idea of how well the unique notion performed. To assess the efficacy of the slurry phase change materials (PCS) (this is a suspended material of micro-encapsulated phase change material (n-eicosane) in water or in a carrier fluid of water and glycol), and contrast it with that of a conformist solar thermal collector, several (dynamic) boundary conditions including the PCM concentration, location, and orientation were used based on a flat-plate solar thermal collector. In this regard, solar energy extraction was utilized as a function of the use of slurry phase change materials. The results of the simulations have demonstrated the resilience of the model and its suitability for use in a recent investigation. Additionally, it was demonstrated that the use of PCS as a heat transfer fluid might boost solar energy extraction to varying degrees, depending on the region. Cold regions can get the biggest benefits.

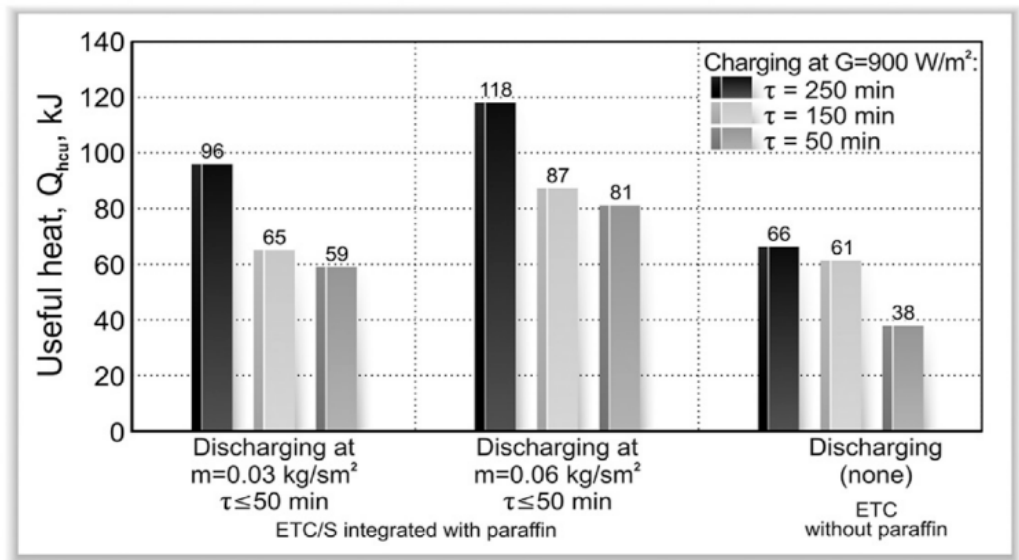


Figure 1. Useful heat is received by the heat collection unit throughout the charge and discharge cycles [25].

In 2017, Li and Zhai [27] presented a solar collector designed for mid-temperature operations. The PCM in this system, which has a melting temperature of 119 °C and is composed of erythritol and expanding graphite, was put within the aluminum pipes before being located inside the evacuated tubes. To conduct heat from PCM to fluid, the heat pipes were occupied in PCM. Based on thermos-physical property tests, the composite PCM with 3 wt% expanded graphite was selected as a good material for heat storage. It should be noted that heat storage was utilized as a function of tube diameter in this study. The thermal performance of this system was then investigated using both the experimental outfit and the computational model. The exposure tests were performed in August, and the analysis revealed that for mid-temperature consumption, the storage performance extended to 40.17%, according to Figure 2. The experimental data also served to verify the numerical model. For heat storage, a phase transition material composed of 3 weight percent expanded graphite and 97 weight percent erythritol is employed. Latent heat, thermal conductivity, and melting point are all 118.69 °C, 312.2 J/g, and 2.4 W/m K, respectively. In comparison to pure erythritol, the addition of expanded graphite improves thermal conductivity by 241.4%.

A hybrid slurry made of microencapsulated phase change materials (MPCMs) of paraffin@melamine resin mixed in an ethanol/water mixture-based multi-walled carbon nanotube (MWCNT) nanofluid was developed and testified by Wang et al. (2019) [28]. Temperature changes in PCM in the cases of charging and discharging were identified as a function of concentration. The study found that when PCM melted and the surface of MPCM exhibited high reflectivity, the temperature rise of the hybrid MPCM-MWCNT slurry was lower than that of pure MWCNT nanofluid in the base fluid (an ethanol/water mixture). However, the final temperatures of the hybrid slurries were higher than those of the MWCNT nanofluid during the thermal discharging phase and increased with the amount of MPCM present. The hybrid slurry comprising 15 wt% MPCMs had a comparable terminal temperature that was approximately 4.6 °C greater than the base fluid, as illustrated in Figure 3.

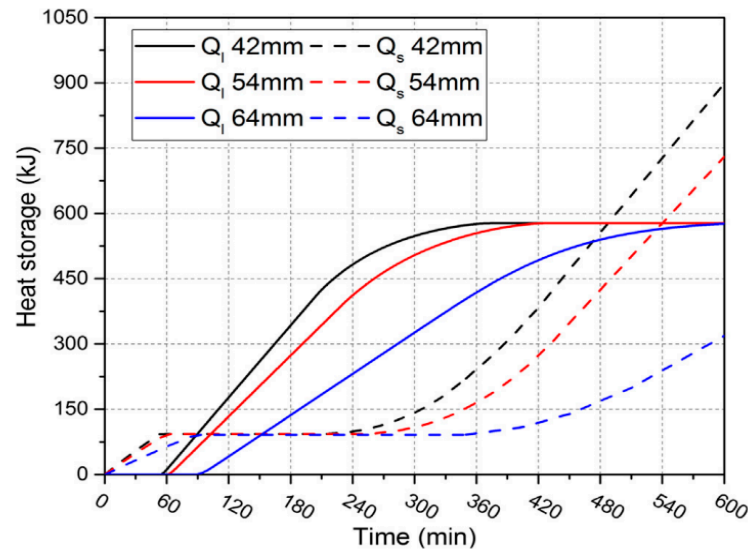
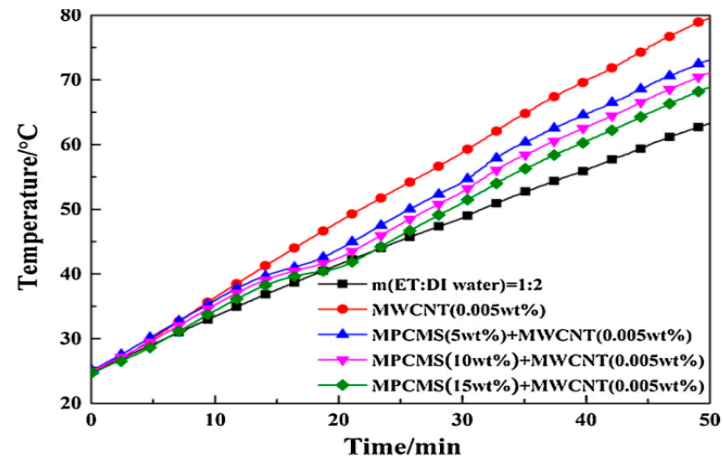
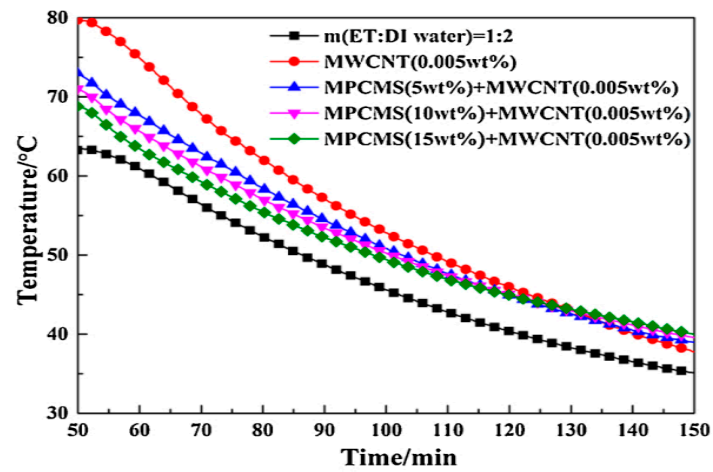


Figure 2. Changes in heat storage with several storage tube diameters [27].



(a)



(b)

Figure 3. Temperature changes in MPCM-MWCNT slurries at two stages of (a) charging and (b) discharging with various concentrations [28].

To overcome the phenomenon of overheating and freezing, a brand-new dual-PCM for flat plate solar collectors was suggested by Wang et al. (2019) [29]. Spherical particles were used to encapsulate the PCM, which comprised 20% high-purity graphite and 80% natural grease. The solar collector contained two layers of PCMs, one with 70 °C of phase change temperature (PCT) and the other with 15 °C of PCT. In other words, the PCM liquefies and absorbs heat when exposed to high temperatures, such as when the water temperature raises the PCM’s high melting temperature above 70 °C. This helps prevent the working fluid from becoming overheated. When the low-melting PCM reaches a temperature of less than 15 °C in a low-temperature situation, the PCM solidifies and releases heat to prevent the working fluid from freezing. Furthermore, this study focused on considering the thermal efficiency of the solar collector as a function of inlet collector temperature. They were positioned in the dual-PCM collector’s area beneath the absorber plate. According to the test results, high-temperature conditions can prolong the time it takes for the absorber plate temperature to rise from 60 to 78 °C by 1.6 h. Further, the dual-PCM collector can be employed to prevent freezing and overheating. Figure 4 shows that the performance of the dual-PCM collector was elevated by 24.1% and 19.6%, respectively, when low-melting PCM was positioned beneath high-melting PCM and the contrary situation.

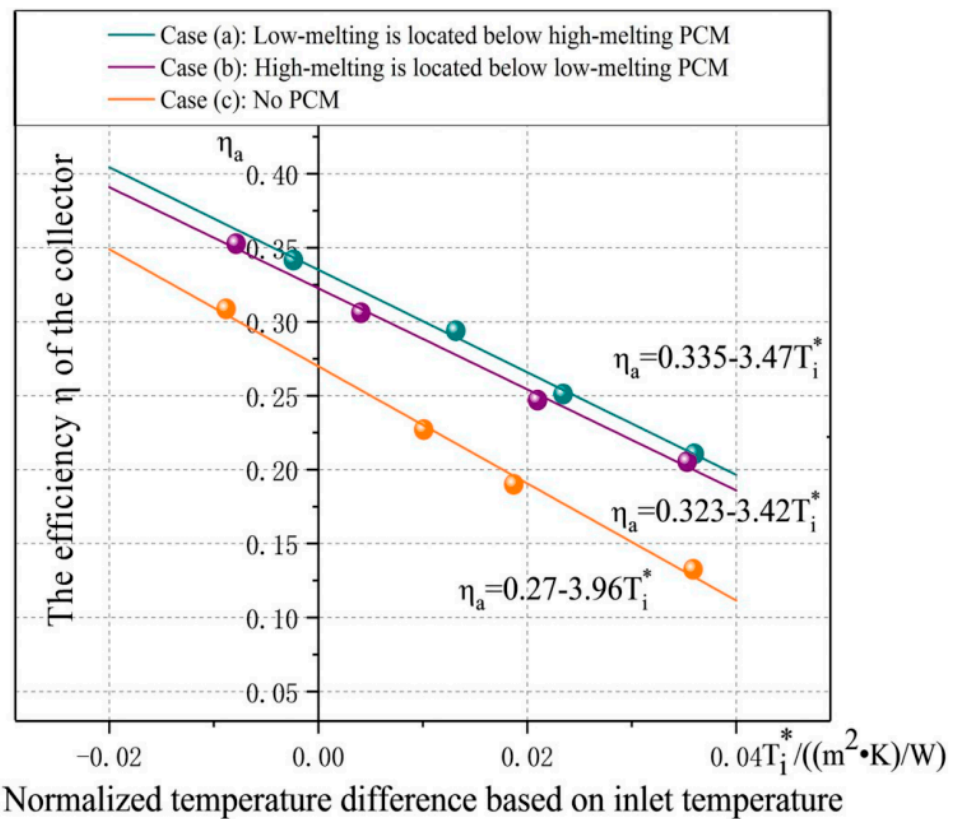


Figure 4. Proficiencies of the PCM collector and conservative collector [29] ($T_i^* = \frac{(t_i - t_a)}{I}$) is the normalized temperature difference based on the inlet temperature $((m^2 \cdot K)/W)$; t_a is the ambient temperature ($^{\circ}C$), I is the solar radiation intensity.)

In situ, polymerization was used by Gao et al. (2020) [30] to create the microcapsule, which had an octadecane core and a melamine-formaldehyde (MF) resin shell that had been amended with a reduced form of commercial graphene oxide (rGO) and oleic acid-coated Fe_3O_4 magnetic nanoparticles in the shell (OA-MNs). In this regard, it is vital to admit that the thermal conductivity of PCM was incorporated as a function of PCM type. According to the experimental findings, introducing rGO significantly improved the thermal conductivity of magnetic PCMs while having no effect on their phase change

activity, as shown in Figure 5. In the meantime, the MF resin shell that functioned as a protective shield significantly increased the thermal stability of octadecane in rGO-MPCMs. The photo-thermal conversion performance was further improved by the rGO-MPCMs slurry's superior optical absorption and thermal storage capabilities compared to MPCMs slurry and deionized water. The rGO-MPCMs in the slurry showed remarkable stability and renewability in the presence of an external magnetic field.

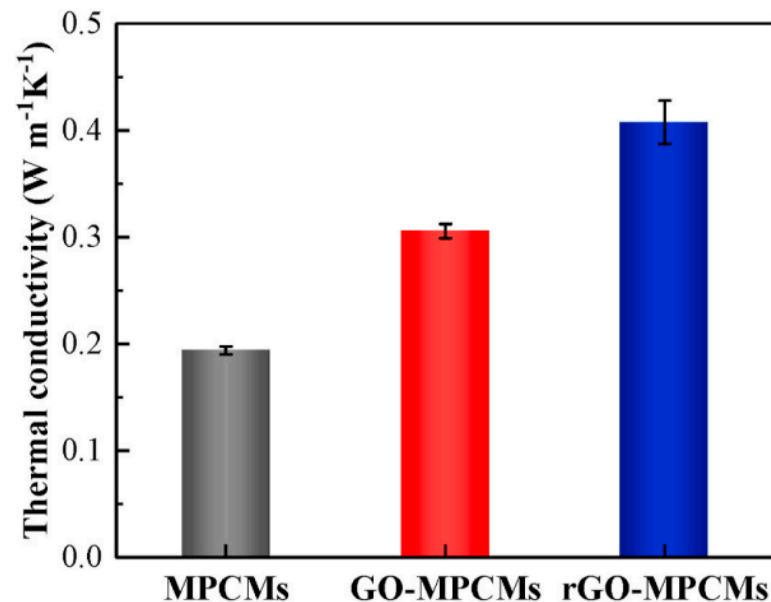


Figure 5. Thermal conductivities of bulk MPCMs, GO-MPCMs and rGO-MPCMs [30].

A detailed comparative examination of a conventional flat plate solar collector (FPSC) and a prototype with an equivalent thermal storage system via PCM was testified by Palacio et al. in 2020 [31]. Experimental and quantitative methods were used to study the devices' thermal performance. An experimental setup measured the temperature of the glass cover, absorber plate, and PCM, in addition to the temperature of the ambient air and the water at the inlet and outflow. Palacio et al. in 2020 [31] introduced the thermal collector efficiency as a function of the contact conduction between the absorber and PCM. With this approach, experimental findings were assessed in order to determine how well both collectors performed under identical operating circumstances. Additionally, several trial scenarios were taken into account to enhance the prototype's thermal efficiency. Analysis was using on two different PCMs (PCM1: Ecopetrol Semirefinada of 60 °C melting point, and PCM2: Rubitherm RT-47 of 41 °C fusion temperature), a contact thermal conduction increase, and collector disposition. According to this study, the contact conduction between the absorber and PCM and the selecting of the PCM are crucial components in enhancing the collector efficacy in comparison to traditional FPSC. Tilting the collector did not significantly improve the latitude of the laboratory investigation.

An innovative evacuated tube solar collector (ETSC) featuring a nano-PCM with fins was proposed and investigated by Elarem et al. 2021 [32]. The effectiveness was examined in relation to the adding of copper (Cu) nanoparticles to paraffin wax. Two PCMs were prepared and tested (PCM1: paraffin wax + 1% nano-Cu, and PCM2: paraffin wax + 2% nano-Cu). The simulation of heat transport through the energy storage process was carried out using ANSYS Fluent (Note: ANSYS is a software that provides a range of simulation capabilities, including structural analysis, fluid dynamics, electromagnetics, and system-level simulations). Last but not least, a set of comparative simulations were run to see how well the ETSC performs with and without the solar parabolic trough reflector (SPTR). In this study, the melting of PCM was identified as a function of fin thickness. It has been concluded that the paraffin phase shift heat transmission in the ETSC was

significantly affected by the addition of fins. The PCM melts more rapidly as a result of lowering the fin thickness. Additionally, adding 1% Cu to the PCM was the appropriate mass concentration for raising the heat transfer fluid output temperature by 2 K, as shown in Figure 6. Additionally, it was found that a final flow rate of 0.003 kg/s was necessary for the PCM’s entire mass to melt. In reality, Nano-PCM can achieve a greater temperature, although briefly. The heat transfer coefficient between the copper tube and the HTF is improved by including Cu nanoparticles into the PCM. The reason for this is because the Nano-PCM filled Evacuated Tube Solar Collector (ETSC) shows improved energy storage during charging, allowing for a longer duration of hot HTF supply during discharging when solar radiation is at its peak.

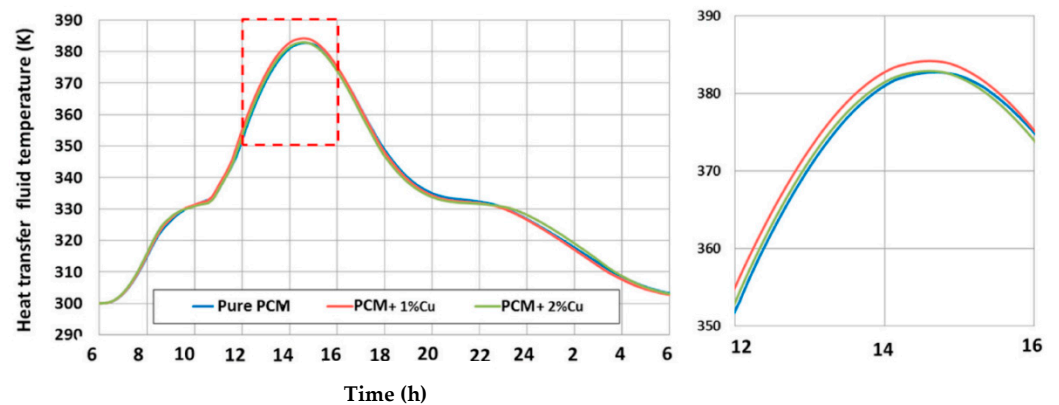


Figure 6. Influence of adding Cu nanoparticles on the heat transfer fluid temperature [32].

The performance of a heat pipe evacuated tube collector (HPETC) with a new approach, which included either one or both evacuated tubes (ET) and two separate storage tanks that incorporated nano- or micro-enhanced PCMs, was analyzed by Alshukri et al. (2021) [33]. The two separate tanks were filled with improved paraffin wax in the suggested designs, whereas ET was occupied with improved medical paraffin wax (grade-A). These two forms of paraffin wax were improved with either ZnO micro-particles or 5 weight percent CuO nanoparticles (MP-ZnO). In this regard, the collector efficiency was expressed as a function of micro or nanoparticle type. The outcomes demonstrated that the combination of improved paraffin wax with NP-CuO and MP-ZnO yields an efficacy enhancement range of 36.8–50% and 25.43–41.4% correspondingly in both ET and the isolated tanks. In contrast to a standard reference collector without PCM, the combination of improved paraffin wax with NP-CuO and MP-ZnO in the only ET increased efficacy with a range of 33.8–45.7% and 23.8–26.7%, respectively, as illustrated in Figure 7.

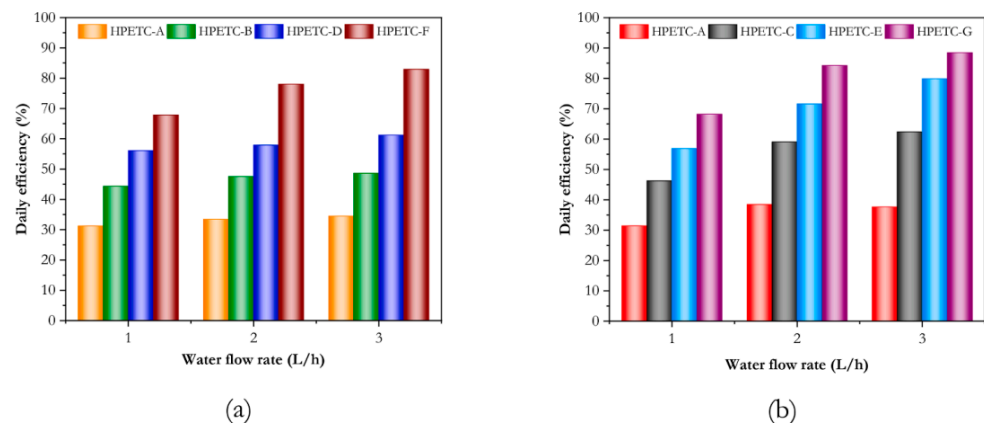


Figure 7. The daily thermal efficiency at three various flow rates for (a) tests 1–3 and (b) tests 4–6 [33].

To overcome the difficulty of solar collectors to immediately store solar energy, Sadeghi et al. (2022) [34] effectively utilized a shape-stabilized phase change material (SSPCM) in a tankless direct-absorption evacuated tube solar collector. The SSPCM utilized in this study consisted of sodium acetate trihydrate (SAT), carboxymethyl-cellulose (CMC), sodium phosphate monohydrate (SPM), and expandable graphite. In this regard, expandable graphite was used to provide the PCM with a shape-stability feature in addition to improving its thermal conductivity. Sadeghi et al. (2022) [34] demonstrated the collector heat gain as a function of flow rate. After determining the appropriate constituent concentrations, the suggested salt hydrate PCM was built utilizing a range of relevant component concentrations and tested through a number of cycles to ensure that it could consistently store heat. The solar system was further refilled in the stagnation mode and then released at flow rates of 10, 27, and 40 (liter per hour) LPH (without water flow). According to the results, the collector-storage system improved thermal efficiency in the stagnation mode from 66% to 82%. Additionally, increasing the flow rate from 10 to 27 LPH did not significantly diminish the heat gain of the collector; however, a decrease in the discharge efficiency occurred after employing a flow rate of 40 LPH.

Yeh et al. (2022) [35] explored a storage-integrated solar thermal collector that had a small footprint and used a compatible phase change material (PCM) for storage. In this study, sodium acetate trihydrate (SAT), a salt hydrate-based composite PCM, was utilized to create a shape-stabilized PCM (SSPCMs) due to its low leakage and excellent thermal conductivity properties. When the built SSPCMs underwent experimental testing, a numerical model was designed to compare the results with the data and estimate the developed SSPCMs' effective thermal characteristics. Furthermore, a model was used to investigate the (dis)charging behavior of a PCM in a storage-integrated solar thermal collector consisting of an evacuated tube and a double-spiral coil heat exchanger. In this regard, the discharging time was illustrated as a function of geometric optimization. With a minimal outlet temperature of 55 °C, a geometrical optimization has been performed to obtain a 2.6-fold longer discharging time. Furthermore, the circulating water is established to be supportive in rising the PCM charging rate by 9% by transporting heat from the surface of the tube to its center.

Nekoonam and Ghasempour (2022) [36] examined the thermal responses of a solar system with thermal energy storage. To address the PCM's low thermal conductivity for energy storage and increase the system's charging and storage efficiencies, a novel technique incorporating the use of sensible-latent materials (encapsulated spherical capsules of PCM and synthetic oil) as the ideal setup with two different options was used (option 1: outlet temperature of the unit with no temperature limitation; option 2: outlet temperature of the unit with threshold restriction). Charging time was considered in this study as a function of the Heat Transfer Fluid (HTF) flow rate. The findings indicated that a 5% rise (reduction) in the input HTF temperature reduced (increased) the charging time by 25% (32%) and enhanced (decreased) the total stored energy by 20% (by 7%). Moreover, a 50% change in the HTF flow rate causes a 12% gain or a 25% drop in charging time. For the first and second optimization scenarios, the best configuration stores 4940 and 4725 kWh of energy during the charge, which is approximately 14% more than the single PCM/sensible investigated situations.

Wen et al. (2022) [37] conducted a detailed performance assessment of an inventive concentrating system made up of a photovoltaic/thermal (PV/T) module with PCM and a solar thermal (ST) collector with thermoelectric generators (TEG) connected in a series. In this technology, the PV/T module produces low-temperature thermal energy in addition to photoelectric power generation, and the ST module and TEG on ST provide the secondary heated water and secondary thermoelectric output. Furthermore, The PV cell's operational temperature can be lowered by the PCM during the day, and the platform can avoid freezing in the winter by releasing heat at night. The electrical and thermal performance were demonstrated in this study as a function of the Fresnel lens. Theoretical analyses revealed that the PV/T-ST system, which consists of a sequence of the ST and T modules,

accomplishes well in terms of thermal and overall performance. Throughout the course of the whole day of activity, the water tank in the PV/T-ST system has a maximum temperature that is approximately 5 °C higher than the PV/T-PV/T system. The electrical and thermal performances using the 1.1-m² Fresnel lens are also 10.65% and 65.22%, respectively, at 12:30. TEG converts some thermal energy into electrical energy over the day, increasing the quantity of high-grade energy in the system by approximately 321.53 kJ.

By using molecular dynamics modelling, Hatamleh et al. (2022) [38] examined the thermal behavior of glass in the vicinity of PCM (decane). In their research, temperature and density profiles were used to examine the atomic behavior of the structure. Furthermore, heat flow and thermal conductivity were used to examine the simulated structure's thermal behavior. The quickly altering of PCM was expressed as a function of the design of the structure. According to the numerical findings, fluid particle density and temperature maximums are 0.09643 atoms/cm³ and 1067.51 K, respectively. The structure exhibits a thermal conductivity of 0.74 W/m K and a heat flow of 650.27 W/m². Overall, incorporating phase change materials in the design can prevent energy loss, lower energy expenses, and facilitate rapid phase changes in the materials, positively impacting the structure's performance.

Algarni et al. (2020) [39] explored whether a novel evacuated tube solar collector (ETSC) concept that incorporates nano-enhanced PCM (Ne-PCM) (0.33 wt% nano-copper with paraffin wax composite) as a latent heat thermal energy storage system could improve the performance of a conservative evacuated tube collector (ETC). This innovative technology combines the U-pipe of the evacuated tube solar collector (ETSC) with the Ne-PCM to form a single unit (ETSC/Ne-PCM) that can generate heat even when solar intensity is limited or inaccessible. By heat accumulation and the thermal insulation of the evacuated tubes, the new system functions as a thermal promoter, extending the time it takes to produce hot water and reducing temperature swings. Additionally, the effectiveness of ETSC was articulated as a function of the weight percent of Cu/PCM. It was discovered that adding 0.33 weight percent of copper/PCM composite to the ETSC increased its effectiveness by 32%. Moreover, the ETSC/Ne-PCM system with 0.08 L/min can deliver hot water up to 50 °C for roughly 2 h longer than standard ETC systems.

Karami et al. (2023) [40] examined the thermal efficiency of CuO nanofluid, CuO/Al₂O₃ binary nanofluid, and CuO nanofluid mixed with micro-encapsulated phase transition material in direct absorption solar evacuated tube collectors (MPCM). To simulate the MPCM slurry, two models—single-phase and mixture—were employed. The single-phase model is advised to shorten calculation time owing to the negligible distinction between the two-phase model's results. The coefficient of performance was justified as a function of the volume % of nanoparticles. It was discovered that 0.06% Al₂O₃ + 0.002% CuO/water nanofluid and 0.06% Al₂O₃ + 0.002% CuO/(ethylene glycol) EG nanofluid, which are equivalent to 28.34 K and 36.64 K, respectively, provide the largest changes in outlet temperature. In both water- and EG-based nanofluids, the collector efficiency utilizing binary nanofluids is greater than that of using CuO nanofluids. According to the observations, the addition of MPCM and CuO nanofluid boosts the coefficient of performance by 4.53% and reduces heat loss by 5.84%. Across all working fluids, the combination of MPCM and CuO nanofluid simultaneously had the maximum accuracy.

A PCM of Trtriacontane paraffin is directly incorporated within the heat pipe evacuated tube solar collector (HPETC) and has copper (Cu) porous metal implanted in was developed by Pawar and Sobhansarbandi (2023) [41]. The performance of the suggested system was contrasted against that of a traditional HPETC system under comparable circumstances in order to make comparisons. Taking into account the distinction of fin temperature, output water temperature, energy, exergy efficacy, and cost analysis, each system's thermal performance was evaluated. The maximum temperature increase was identified as a function of PCM and Cu porous that fill the evacuated tube. The results demonstrated that the evacuated tube filled with PCM + Cu porous metal was able to reach a maximal temperature increase of approximately 21 °C when solar radiation was at its highest amount. The difference in fin temperature between the ordinary evacuated tube

and the evacuated tube filled with PCM + Cu porous metal was observed to be 36.1 °C after sunset. Additionally, on 9–11 April, at 10 PM, the highest water outlet temperature differences of 8 °C, 10 °C, and 11 °C, respectively, were discovered between the two designs. The conventional system only recorded a daily energy efficiency maximum of 36.91%, but the suggested scheme showed a maximum energy efficiency of 85.64%.

Studies on phase transition materials for solar collectors are shown in Table 1. Specifically, Table 1 introduces details of configurations, type of study, studied parameters and highlights the most important findings for those studies approximately solar collectors.

Table 1 can show that the ETSC's efficacy was found to rise by 32% with the use of 0.33 weight percent of copper/PCM composite. The prototype with a PCM raised the night outlet temperature by 2 °C and improved the greatest gathered energy by 630 Wh, if compared to the collector without a PCM. By using this collector-storage system, the thermal efficiency during stagnation mode increased from 66% to 82%.

2.2. Solar Still-Related Studies

A solar still system is a device that evaporates and condenses water to purify it using sun energy. A solar still's basic structure consists of a shallow basin or trough with a transparent cover, typically made of glass or plastic, that lets sunlight in and warms the water inside. Water vapor rises and condenses on the bottom of the lid as it evaporates, gathering there to be collected in a different container [42]. A solar still's effectiveness is affected by a number of variables, including the quantity of sunshine it receives, the surface area of the basin, the material used for the cover, and the temperature and humidity of the surrounding air [43]. For maximum effectiveness and system longevity, the system must be properly maintained, which includes routinely cleaning the basin and cover. In places where access to clean water is scarce or non-existent, solar still systems can offer a low-cost, long-term alternative for producing drinkable water.

This section attempts to provide a comprehensive review of recent studies that encountered the implications of PCMs in solar stills with a critical analysis of the overall performance.

Using a new shape-stabilized phase change material (SSPCM), Cheng et al. (2019) [44] provided an original experiment as well as a simulation model to assess the efficiency of solar still. SSPCM of 5 wt% expanded graphite was specifically used. High thermal conductivity, a steady form, and strong sun absorption were all characteristics of the SSPCM. The SSPCM employed in the investigation had a thermal conductivity of 1.50 W/m K and a solar absorption of 0.94, making it a suitable replacement for the traditional metal absorber plate. Next, a test for solar still with PCM (SSPCM) was conducted. According to the trial findings, as depicted in Figure 8, the SSPCM's daily productivity was 3.41 L/m², 43.3% greater than that of the traditional solar still without PCM. The modeling findings demonstrated that when the thermal conductivity of SSPCM improved from 0.2 to 4.0 W/m K, the daily production rose from 42% to 53% compared to that of traditional solar still. The proportion of boosting productivity augmented from 21.5% to 57.5% as the melting temperature of SSPCM rose from 34 to 50 °C.

Vigneswaran et al. (2019) [45] conducted an investigation to appraise the thermal efficiency of three passive solar stills of the same size. The first still was a conventional solar still (Still I), the second was a still with a single PCM (paraffin wax) (Still II), and the third was a still with two PCMs (Still III). The two PCMs utilized in Still III had different temperature ranges for their phase change but similar capacities for latent heat storage. PCM1 and PCM2 had a temperature range for a phase change of 58.03 °C to 64.5 °C and 53.05 °C to 62 °C, respectively. The tests were achieved in Chennai, India from February to May. PCM1 was designed to discharge stored latent heat energy once the solar radiation began to diminish, while PCM2 was intended to discharge heat when PCM1 had almost discharged all the stored energy. The researchers analyzed the thermal performance of the three stills in terms of hourly yield day⁻¹ and exergy performance. The yields of Stills I, II, and III were 3.680, 4.020, and 4.400 L/m²/day, respectively.

Table 1. Outline of studies on phase change material for solar collectors.

Authors (Year) [Reference]	Configuration/Composition	Type of Study	Studied Parameters	Highlighted Results/Findings
Feliński and Sekret (2016) [25]	A system that combines an evacuated tube collector with a PCM storage unit.	Experimental	Effect of using PCM.	The paraffin-integrated ETC/S system produced a total improvement of 45–79% in usable heat.
Serale et al. (2016) [26]	Location, orientation, and PCM concentration were implemented to appraise the efficacy of the PCS-based technology.	Experimental	Effect of PCS as a heat transfer fluid.	Depending on the climate, the use of PCS as a heat transfer fluid can boost solar energy extraction to varying degrees.
Li and Zhai (2017) [27]	Before being inserted into the evacuated tubes, the aluminum pipes were filled with PCM made of erythritol and expanding graphite.	Numerical and experimental	Impact of using PCM.	Using PCM led to enhancing the storage efficacy by 40.17% for mid-temperature utilization.
Wang et al. (2019) [28]	Hybrid slurries containing MPCMs dispersed in ethanol/water-based multi-walled carbon nanotube (MWCNT) nanofluid are used.	Experimental	Impact of hybrid MPCM-MWCNT slurry.	Compared to the base fluid, a combination of ethanol and water, the temperature increase in the hybrid MPCM-MWCNT slurry was less.
Wang et al. (2019) [29]	A novel dual PCM in flat plate solar collector.	Experimental	Impact of A novel dual PCM.	When low-melting PCM was positioned beneath high-melting PCM and when the conditions were reversed, the dual-PCM collector’s performance rose by 24.1% and 19.6%, respectively.
Gao et al. (2020) [30]	Microcapsule, with melamine-formaldehyde resin shell and octadecane core.	Experimental	Effect of adding rGO.	The inclusion of rGO significantly increased the thermal conductivity of microcapsules containing magnetic phase change material.
Palacio et al. (2020) [31]	A traditional flat plate solar collector and a corresponding prototype equipped with a thermal storage system using PCM.	Experimental	Effect of using PCM.	In comparison to the collector without a PCM, the prototype with a PCM raised the night outlet temperature by 2 °C and improved the maximum gathered energy by 630 Wh.
Elarem et al. (2021) [32]	Evacuated tube solar collector integrating a nano-PCM with fins.	Numerical	Effect of using fins and nanoparticles on the PCM.	The inclusion of fins has a major influence on the paraffin phase transition heat transfer in the ETSC. The PCM melts more rapidly as the fin thickness decreases. Additionally, it was discovered that 1% Cu fed to the PCM was the optimal mass concentration for a 2 K rise in the HTF outlet temperature.

Table 1. *Cont.*

Authors (Year) [Reference]	Configuration/Composition	Type of Study	Studied Parameters	Highlighted Results/Findings
Alshukri et al. (2021) [33]	A new method of integrating nano- or micro-enhanced PCMs was applied to an evacuated tube collector, which included one or both evacuated tubes and two separate storage tanks.	Experimental	Effect of improved paraffin wax with NP-CuO and MP-ZnO.	For an evacuated tube, the addition of improved paraffin wax with NP-CuO and MP-ZnO increased efficiency by a range of 33.8–45.7% and 23.8–26.7%, respectively.
Sadeghi et al. (2022) [34]	A tankless direct-absorption evacuated tube solar collector was successfully applied with a shape-stabilized PCM.	Experimental	Effect of shape-stabilized PCM.	This collector-storage system increased the thermal performance in the stagnation mode from 66% to 82%.
Yeh et al. (2022) [35]	Storage-combined solar thermal collector and its compatible PCM.	Experimental and numerical	Impact of PCM.	The PCM charging rate is observed to increase by 9% thanks to the circulating water’s ability to transfer heat from the tube’s surface to its interior.
Nekoonam and Ghasempour (2022) [36]	Solar system with thermal energy storage.	Numerical	Effect of configuration.	The optimum configuration retains at approximately 14% more energy during charging than the single PCM/sensible cases, at 4940 and 4725 kWh for the first and second optimization scenarios, respectively.
Wen et al. (2022) [37]	Photovoltaic/thermal module with PCM and a solar thermal collector with thermoelectric generators connected in series.	Experimental and numerical	Effect of configuration.	Thermal and overall performance are both strong points of the PV/T-ST system, which integrates the ST and PV/T modules in series.
Hatamleh et al. (2022) [38]	Molecular dynamics simulation was used to investigate the behavior of glass in the presence of decane PCM.	Numerical	Effect of using PCM.	While fast changing the phase of the materials, phase change materials can limit energy loss, lower energy expenditures, and improve a building’s aesthetic.
Algarni et al. (2020) [39]	Evacuated tube solar collector integrating nano-enhanced PCM.	Experimental	Impact of copper/PCM composite.	The ETSC was shown to be 32% more effective when 0.33 weight percent of copper/PCM composite was added. Furthermore, due to its particular mass flow rate of 0.08 L/min, the ETSC/Ne-PCM can provide hot water for up to 2 h longer than conventional ETC systems, with temperatures reaching up to 50 °C.

Table 1. Cont.

Authors (Year) [Reference]	Configuration/Composition	Type of Study	Studied Parameters	Highlighted Results/Findings
Karami et al. (2023) [40]	Using CuO nanofluid, CuO/Al ₂ O ₃ binary nanofluid, and CuO nanofluid coupled to microencapsulated PCM, direct absorption solar evacuated tube collectors are used.	Numerical	The influence of water and ethylene glycol and nanofluid volume fraction.	The effectiveness of the collector is increased by 4.53% and the energy loss is decreased by 5.84% when MPCM and CuO nanofluid are combined.
Pawar and Sobhansarbandi (2023) [41]	A PCM embedded with copper porous metal which is incorporated within the HPETC.	Experimental	Impact of a PCM embedded with copper porous metal.	The evacuated tube filled with PCM + Cu porous metal had a rise in maximum temperature of almost 21 °C.

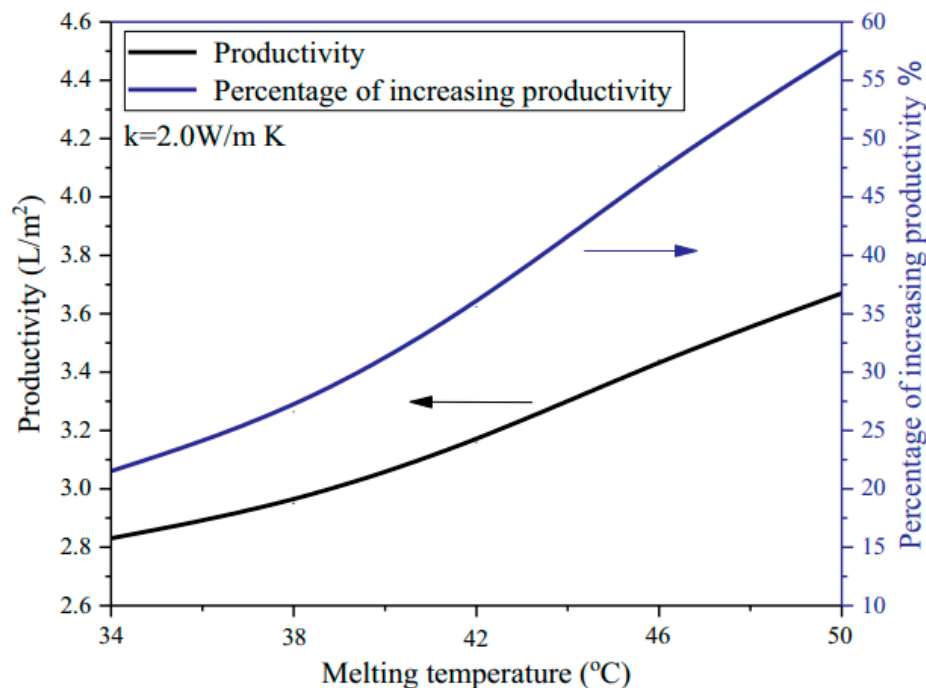


Figure 8. The daily output and the increase in daily output of the shape-stabilized PCM (SSPCM) with various melting temperatures [44].

Abu-Arabi et al. (2020) [46] conducted a study to evaluate the efficiency of adapted solar still under different scenarios. The solar still was modified and tested in three options: SC connected to an external collector (SCC), solar still with glass cooling (SC), and SCC with PCM (SCCP). In this regard, three PCMs utilized: sodium thiosulfate pentahydrate, sodium acetate trihydrate, and paraffin wax. The results showed that the productivity of the SC, SCC, and SCCP systems (with SAT as PCM) increased from 0.9 to 3.4 mL/min, 2.35 to 10 mL/min, and 3 to 11.9 mL/min, respectively. This is specifically conducted increased from 200 to 700 W/m². The adding of an external collector and PCM improved productivity by 2.4 fold. An increase in the coolant mass flow rate from 0 to 10 kg/s has caused an increase in productivity for all systems. Moreover, an increase in the hot water circulation rate of the external collector has also increased productivity for the SCC and SCCP systems. The best PCM was the one with the greatest melting point and latent heat of fusion, and the ideal mass ratio of basin water to PCM was 2:1.

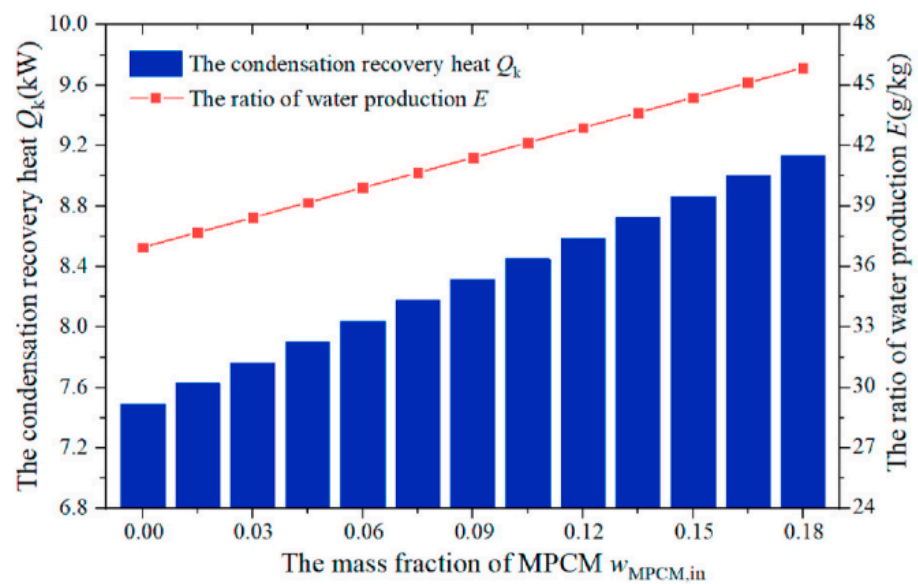
Incorporating hollow cylindrical pin fins was proposed by Yousef et al. (2019) [47] to improve the heat transfer properties of a PCM storage unit used in a solar still system. These fins functioned as thermal conductivity enhancers (TCEs). The study considered three scenarios: Case 1, a conservative solar still without PCM; Case 2, a solar still with PCM; and Case 3, a solar still with a pin-finned heat sink embedded in the PCM. The efficiency of each scenario was assessed and compared through experimental evaluation under the same climatic conditions. The findings elucidated that the existence of PCM had a negative impact on daytime freshwater productivity, but overall freshwater yield increased significantly. Moreover, the solar still with pin-finned PCM (Case 3) demonstrated superior thermal efficiency compared to both the conservative still (Case 1) and the solar still with only PCM (Case 2). The total daily water productivity was found to be 17% and 7% higher in Case 3 than in Cases 1 and 2, respectively. Additionally, the study showed that the inclusion of PCM in Cases 2 and 3 extended the productivity of distilled water after sunset by roughly 5 and 7 h, respectively.

A unique PCM tube shape was created by Elashmawy et al. (2020) [48] for usage within a tubular solar still with a parabolic solar concentrator. Twelve aluminum tubes with paraffin wax within each serve as a PCM. To improve the thermal qualities, copper

rods are placed inside the paraffin wax. The tubular solar still is exposed to stronger sun radiation thanks to a parabolic concentrator solar tracking device. The experimental work was carried out in Ha'il City, Saudi Arabia, which is located at 27.64° N and 41.75° E and is 965 m above sea level. After being coated black, the 12 aluminum tubes were put within the trough. The productivity and device performance in freshwater has significantly improved, with comparatively low production costs. The productivity and performance of the created device are improved by 40.51% and 38.25%, respectively, when PCM tubes are used. When utilizing a device with PCM tubes, the yield, efficiency, and cost per liter are 5.55 L/m² day, 44.1%, and 0.00782 USD, respectively. In contrast, using a device without PCM tubes yields 3.95 L/m² day, 31.9% efficiency, and a cost of \$0.0163 USD per liter.

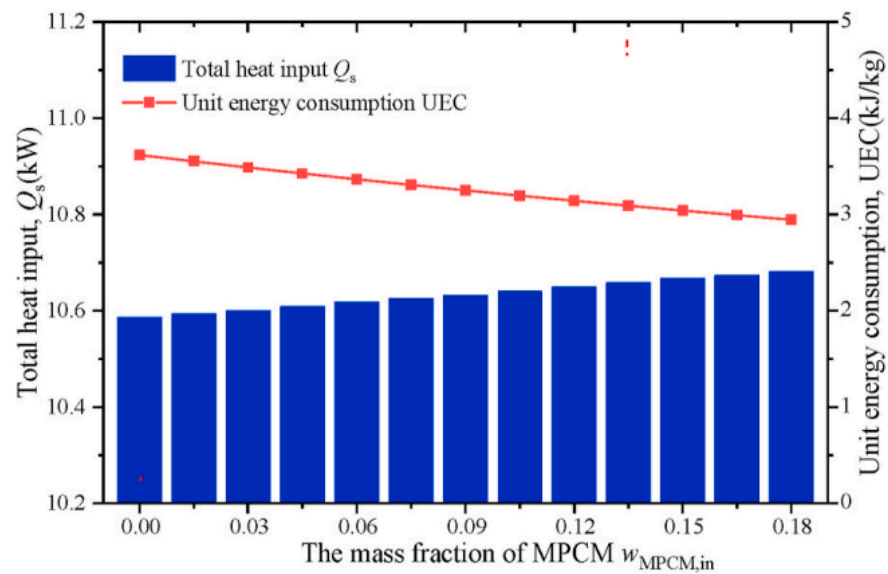
Kabeel et al. (2020) [49] conducted experiments to elevate the efficiency of tubular solar still during both daytime and nighttime. They achieved this by adding enhancements to the design and construction, specifically by constructing closed copper tubes filled with PCM (paraffin wax), which suited the basin of the still. The enhancements led to a noteworthy rise in the production of distilled water, where conventional tubular stills produced 4.1–4.31 L/m²/day, while utilizing closed copper tubes filled with PCM increased productivity to 8.82–9.05 L/m²/day during June–August 2019, resulting in a 110–115.1% increase in accumulated productivity under similar conditions. Moreover, daily efficiency also improved, with conventional tubular stills achieving between 32.9% and 33.8%, whereas the utilization of closed copper tubes filled with PCM increased daily performance to 70.9–72.7%, representing a 114.4–115.5% increase in daily performance. Overall, the outcomes demonstrated that the use of copper tubes filled with PCM is a promising option for achieving optimal performance in tubular solar stills.

Solar-driven-spray flash evaporation (SFE) desalination unit improved using latent heat fluids was reported by Chen et al. in 2021 [50]. The addition of microencapsulated MPCM (TH-ME 58 (SiO₂-paraffin)) in a NaCl aqueous solution improves the working fluid's thermal energy storage and SFE process. The simulation results indicate that the use of MPCM in droplets can delay the temperature drop during the flash evaporation process due to their higher effective heat capacity. By adding 0.18 mass fraction of MPCM to the flash evaporation fluid, the water production ratio increased by 23.1%, and the specific energy consumption reduced by 18.3%. This is clearly depicted in Figure 9.



(a)

Figure 9. Cont.



(b)

Figure 9. SFE-condensation efficiency for different added solutions of different mass fractions of MPCM (a) the ratio of water production; (b) unit energy consumption [50].

Jahanpanah et al. (2021) [51] studied the impact of low-temperature PCM on the overall efficiency and productivity and basin temperature in a single-slope solar still. A commercialized inorganic salt hydrate + water + Additive PCM (Product number: PGSCR Co. PCM28/315) of 28 °C melting point, low temperature, and latent heat of fusion of 225 kJ kg⁻¹ was chosen for this objective as a cutting-edge method in the industry. Investigations were conducted on three cases: (1) still without PCM, (2) still with 3 kg of PCM, and (3) still with 6 kg of PCM. The operative temperature, hourly and collective productivities, and desalination effectiveness were all observed and computed throughout each experiment. It was discovered that the addition of 6 kg of PCM can raise desalination efficiency from 28.13% to 36.42% while improving production overall by 30.3% (Figure 10). The outcomes demonstrate that the performance of the solar stills might be effectively enhanced by the use of low-temperature PCMs.

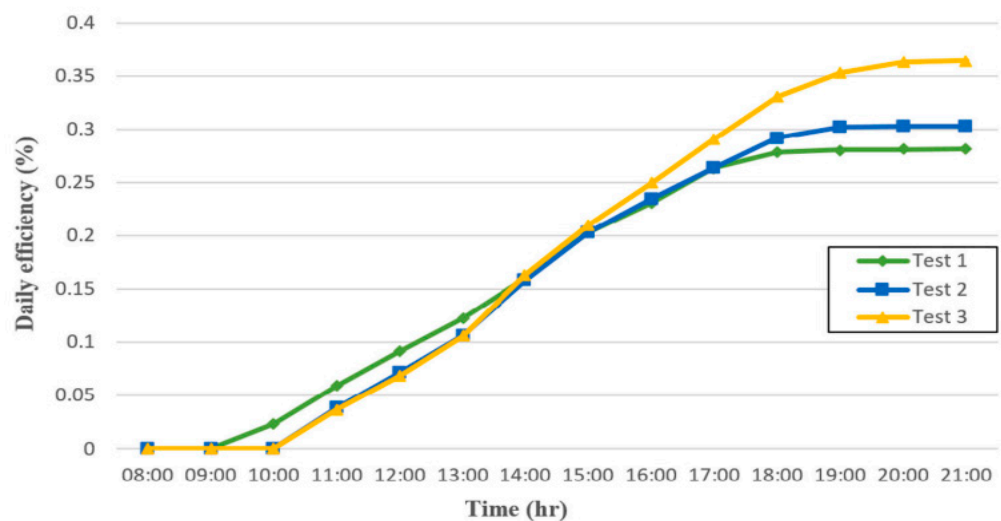


Figure 10. Daily desalination efficiency of the unit for three test cases [51].

In a study conducted by Gnanavel et al. (2021) [52], the efficiency of solar still was enhanced by incorporating a PCM. The experimental setup consisted of an aluminum basin with and without the phase change material, and tests were conducted from 7 a.m. to 6 p.m. to determine hourly and cumulative productivity. Trimethylolthane and paraffin C18 were used as PCMs, and the results indicated that paraffin C18 resulted in greater productivity. CFD analysis was performed to validate these findings.

The inclined and traditional solar stills were coupled by Hansen et al. (2022) [53] to increase the daily distillation yield as a whole. Both stills store latent heat through the use of paraffin wax. In the course of the day, the PCM stores thermal energy and releases heat as needed. The solar still's productive yield throughout the night is provided by the thermal energy storage of latent heat. The solar still is connected with external add-ons such as flat, steeped, and fin-shaped absorbers to improve distillation. The experiment was conducted outside, and daily production was assessed. This study determined that fin-shaped absorbers were more productive, and it was combined with PCM to produce a supreme amount of 5.62 L/day of distillate. The inclined still with the fin-shaped absorber was shown to be more creative when paired with basin still, with a production increase of 74.5%, and when coupled to PCM and basin still, with an increase in productivity of 87.96%.

Ajdari and Ameri (2022) [54] constructed an inclined stepped solar still with baffles to study the impact of the input brine flow rate, CuO/graphene oxide (GO) nanocomposite weight percent, a volume ratio of individual nanoparticles in the nanocomposite, existence of paraffin wax as a PCM, and distillate yield on the glass, brine, and bottom temperatures. As a consequence, the freshwater yield increased by 48.12 and 81.59%, respectively, with 0.03 wt% CuO and GO. Freshwater volume rose by 81.59%, thanks to a nanocomposite with a volume ratio of 30/70 for CuO/GO. Additionally, it was discovered that reducing the brine flow rate from 30 to 8 Lh⁻¹ enhanced the productivity of freshwater while raising it to 68 Lh⁻¹ decreased the distillate yield. Last but not least, adding paraffin wax as PCM to the solar still's stages increased distillate production by 32.8%. In conclusion, it is shown that the CuO/GO nanocomposite is a promising alternative to be used in solar stills to elevate their productivity.

Abdullah et al. (2022) [55] carried out an experimental investigation to enhance the efficiency of the Tray Solar Still (TSS). The rate of heat transfer between the TSS absorber and the saline water has improved. The effectiveness of TSSs with flat and finned absorber forms was therefore examined. Conventional solar stills (CSS), TSS, and finned TSS were the SSs that were examined (FTSS). The finned absorbers were covered with jute wick materials, allowing water from the wick feed to gently rise through the porous material. PCMs of paraffin wax combined with copper oxide nanoparticles have been used to examine the FTSS efficiency for further improving TSS efficiency. The water basin has also been heated using three electric heaters. To occupy the same space as the FTSS and function as a power supply for electric heaters, a photovoltaic cell was constructed adjacent to the back wall of the FTSS. According to the results, using heaters and PCMs with nanoparticles increased FTSS productivity by 166 and 136% as contrasted to that of the CSS, respectively. Moreover, employing electrical heaters and PCMs with nanoparticles simultaneously increased the FTSS's daily water productivity by 196% over the CSS.

By adding an internal sidewall reflector, hollow circular fins, and a nanoparticle-PCM, Tuly et al. (2022) [56] improved the efficiency of actively modified double-slope solar distiller units. One standard still and four modified stills with the specified connections were utilized in the experiment. According to the findings, the solar still modified with a reflector, fins, and nano-PCM produced a max of 1853 mL per day. The system's most efficient adaptation was discovered to be the employment of a paraffin wax-Al₂O₃ nanoparticle mixture (paraffin wax and 3 wt% Al₂O₃), which offered nearly twice as much cumulative productivity as the pure PCM (just paraffin) scenario. In the situations of pure PCM and nano-PCM, distillate accumulation was superior to the conventional scenario by 61.36% and 92%, respectively. In addition, the combined effect of the circular fin, reflector, and nano-PCM resulted in achieving the highest energy efficiency of 21.56%.

A combined double-slope solar still (DSSS) and PCM-TES were proposed by Afolabi et al. in 2023 [57]. Using vacuum mold-filling processes, PCM was microencapsulated in an epoxy resin composite. Specifically, they used 1.5 wt% of 40 nm sized Zn-nanoparticle and 5 kg paraffin PCM. To determine the impact of TES on productivity, the collected data from the traditional DSSS and DSSS-TES have been evaluated. The DSSS-TES system attained average daily temperatures of 65.2 °C, 77.5 °C, 82.4 °C, 79.5 °C, and 68.4 °C for the glass cover, humid air, salt water, still basin absorber, and TES cavity, respectively. With 7.5 L of potable water every day and a 3 h expansion of the working period, DSSS-TES has produced more. Moreover, rates of condensation and evaporation surged by 105% along with the rise in production. The system's integration of TES has decreased heat losses, and a microencapsulated insulator has stopped PCM nanocomposite leakages. Desalinated water has not been discovered to contain any metals, microbes, or organic pollutants.

Bacha et al. (2023) [58] introduced an inventive design for tubular solar distillers that enhances productivity while minimizing costs. This was accomplished by replacing the flat absorber with a convex one covered in black jute wick material and incorporating an energy storage reservoir containing paraffin wax beneath the convex absorber. An oil heat exchanger was also included with a solar parabolic concentrator serving as an additional heat source. The effectiveness of this new design was assessed through the creation of two tubular solar distillers and conducting tests in Al-Kharj, Saudi Arabia. The first distiller was a standard tubular solar distiller used as a control, while the second was a modified convex tubular solar distiller (MCVTSD). The outcomes demonstrated the superior productivity of the MCVTSD, which achieved 13.58 L/m²/day. Furthermore, the pioneering configuration has upgraded thermal and exergy efficiencies, and overall productivity by 39.32%, and 4.99%, 233.25%, respectively, compared to the conventional tubular solar distiller.

The evaluation of the studies described in Table 2 shows that the joint effects of circular fin, reflector, and nano-PCM result in a maximum energy efficacy of 21.56%. The overall freshwater yield still significantly increases as a result of PCM, which also has a detrimental effect on daytime freshwater productivity. Moreover, productivity was boosted by 2.4 fold with the inclusion of PCM and an external collector.

2.3. Solar Pond-Related Studies

A solar pond system is a device that employs a sizable, shallow pond to gather and store solar energy for use in heating and electricity production, among other things. A solar pond's basic structure is made up of a number of salt concentration-varying layers that together form a gradient that traps solar energy and warms the water at the pond's bottom. The heated water can subsequently be used for a variety of purposes, including the production of energy through a turbine, heating of enclosed spaces, and industrial activities. The depth of the pond, the gradient in salinity, the amount of solar radiation, and the surrounding temperature all have an impact on how well a solar pond performs [59]. By choosing the right pond shape and size, maximizing the salinity gradient to optimize thermal stratification, and properly insulating the pond, one can increase the efficiency of a solar pond system [60]. For the system to operate at its best and last as long as possible, it must be properly maintained, which includes monitoring the salinity gradient and routinely clearing the pond of sediment and other waste. Particularly in regions with plenty of sunlight and restricted access to conventional energy sources, solar pond systems can offer a low-cost, environmentally friendly solution for producing thermal energy in a range of applications.

The current section provides a valuable summary of the associated research on PCMs in solar pond systems.

Table 2. Outline of studies on phase change material for solar still.

Authors (Year) [Reference]	Configuration	Type of Study	Studied Parameters	Highlighted Results
Cheng et al. (2019) [44]	Solar still with using a new shape-stabilized phase change material (SSPCM).	Experimental	Effect of SSPCM in solar still.	The solar still utilizing SSPCM demonstrated a daily output of 3.41 L/m ² , indicating a productivity increase of 43.3% compared to the standard solar still without SSPCM.
Vigneswaran et al. (2019) [45]	Solar stills with three different configurations were tested: a conventional solar still (Still I), a solar still with a single phase change material (Still II), and a solar still with two PCMs (Solar III).	Experimental	Impact of using PCM.	The yield of Still I was 3.680 L/m ² /day, while Still II and III produced 4.02 and 4.4 L/m ² /day, respectively. The productivity of Still III was 4.40 L/m ² /day, representing a 19.6% and 9.5% increase in yield compared to Still I and II, respectively.
Abu-Arabi et al. (2020) [46]	Solar still, solar still linked to a third-party collector, and solar still with glass cooling with PCM. The three PCMs—sodium thiosulfate pentahydrate, paraffin wax, and sodium acetate trihydrate—were all different.	Experimental	Effect of external collector and PCM.	The productivity was boosted by 2.4 fold with the inclusion of the external collector and PCM.
Yousef et al. (2019) [47]	Hollow cylindrical pin fins are included in PCM.	Experimental	Effect of using hollow cylindrical pin fins incorporated into PCM.	The overall freshwater yield still significantly increases when PCM is present, which has a negative impact on daytime freshwater productivity. The cumulative daily yield of distilled water in Case 3 is 17% and 7% higher than that of Case 1 and Case 2, respectively.
Elashmawy et al. (2020) [48]	The PCM used in the solar still consists of paraffin wax filled inside 12 aluminum tubes.	Experimental	Using paraffin wax in 12-aluminum tubes.	The productivity and efficiency of the created device are improved by using PCM tubes by 40.51% and 38.25%, respectively.
Kabeel et al. (2020) [49]	Closed copper tubes filled with PCM were assembled and fixed in the basin of tubular solar still.	Experimental	Impact of closed copper tubes filled with PCM.	The daily performance of traditional tubular still varies between 32.9 and 33.8%, but when closed copper tubes filled with PCM are used, the daily performance increases to 70.9 to 72.7% with an increase of 114.4 to 115.5%.
Chen et al. (2021) [50]	NaCl aqueous solution with the inclusion of PCM in microcapsules.	Experimental	Impact of using MPCM.	Due to their greater effective heat capacity, droplets with MPCM may experience a slower temperature drop during the flash evaporation process. The inclusion of MPCM with a mass fraction of 0.18 into the flash evaporation solution resulted in a 23.1% increase in the water production ratio.
Jahanpanah et al. (2021) [51]	PCM enhanced single-slope solar still.	Experimental	Impact of using PCM in a single-slope solar still.	The addition of 6 kg of PCM might boost output by 30.3% overall and boost desalination efficiency from 28.13% to 36.42%.

Table 2. *Cont.*

Authors (Year) [Reference]	Configuration	Type of Study	Studied Parameters	Highlighted Results
Gnanavel et al. (2021) [52]	Solar still uses phase change materials.	Experimental	Impact of using paraffin 18.	Paraffin C18 material produces more productivity. Paraffin C18 material produces 209.5% more productivity than the case without using paraffin C18.
Hansen et al. (2022) [53]	Paraffin wax is used in the inclined and conventional solar still.	Experimental	Impact of the fin-formed absorber and PCM.	The inclined still with a fin-shaped absorber was particularly productive, with productivity increases of 74.5% when paired with a basin still and 87.96% when combined with PCM and a basin still.
Ajdari and Ameri (2022) [54]	The water production ratio experienced a 23.1% increase when MPCM with a mass fraction of 0.18 was added to the flash evaporation solution. stepped solar still with baffles.	Experimental	Effect of using a nanocomposite in solar still.	The volume of the freshwater was enhanced by 81.59% using a nanocomposite with a volume ratio of 30/70 for CuO/GO.
Abdullah et al. (2022) [55]	PCMs with nanoparticles are used in solar still.	Experimental	Effect of PCMs mixed with copper oxide-nanoparticles.	Using heaters and PCMs with nanoparticles increased the FTSS productivity by 166 and 136% as contrasted to that of the CSS, respectively.
Tuly et al. (2022) [56]	By combining the effects of an internal sidewall reflector, hollow circular fins, and a phase change material mixed with nanoparticles, active modified double-slope solar distiller units are created nano-PCM.	Experimental	Effect of internal sidewall reflector, hollow circular fins, and nanoparticle PCM.	The mutual effect of the circular fin, reflector, and nano-PCM results in the greatest energy efficiency of 21.56%. The mutual effect of the circular fin, reflector, and nano-PCM results in the greatest productivity efficiency of 21.56%.
Afolabi et al. (2023) [57]	Double-slope solar is still integrated with PCM-TES.	Experimental	PCM.	The condensation and evaporation index rose by 105% along with the rise in production. The system's integration of TES has minimized heat losses, and a microencapsulated insulator has stopped leaks from the PCM nanocomposite.
Bacha et al. (2023) [58]	Use a convex absorber rather than a flat one, cover it with black jute wick material, and use a paraffin wax-filled energy storage reservoir beneath the convex absorber.	Experimental	The impact of utilizing a convex absorber, wick materials, and PCM reservoir in conjunction with a solar parabolic concentrator.	The MCVTSD's high productivity was 13.58 L/m ² /day. In this case, MCVTSD's novel design increased productivity and thermal and energy efficiency in comparison to CTSD by 233.25%, 39.32%, and 4.99%, respectively.

Sarathkumar et al. (2017) [61] added Al_2O_3 nanoparticles to PCM to enhance the performance of the solar pond. Al_2O_3 nanoparticles have strong thermal conductivity, and PCM has good heat absorption ability. The time required for solar pond charging and discharging can be greatly decreased, and the rate of heat transfer can be boosted, by the addition of Al_2O_3 nanoparticles. The copper tube contains a mixture of PCM and Al_2O_3 nanoparticles. This encapsulation, which consists of PCM mixed with nanoparticles, is positioned in the pond's LCZ (lower convective zone). In the LCZ, a heat exchanger extracts heat. Power plants can be provided with useful steam to produce electricity. The most usable heat that may be produced is 167 W. Just until evening 6.00 PM could the solar pond without nanoparticles supply water at a warmer temperature. Yet, the solar pond containing Al_2O_3 nanoparticles was capable of providing hot water until 7.30 PM in the evening. As illustrated in Figure 11, the solar pond containing Al_2O_3 particles was still capable to produce hot water for 1.5 h after sunset.

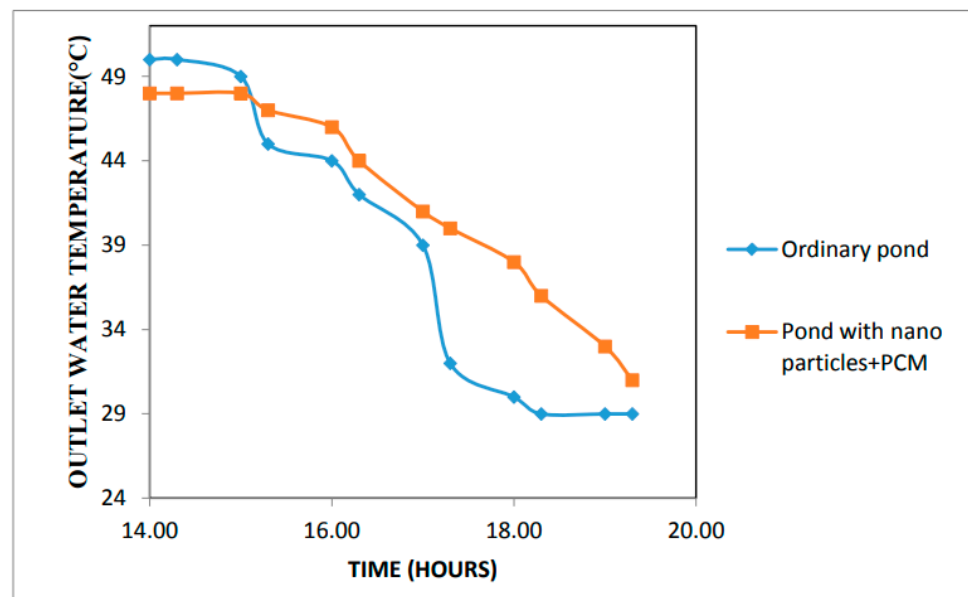
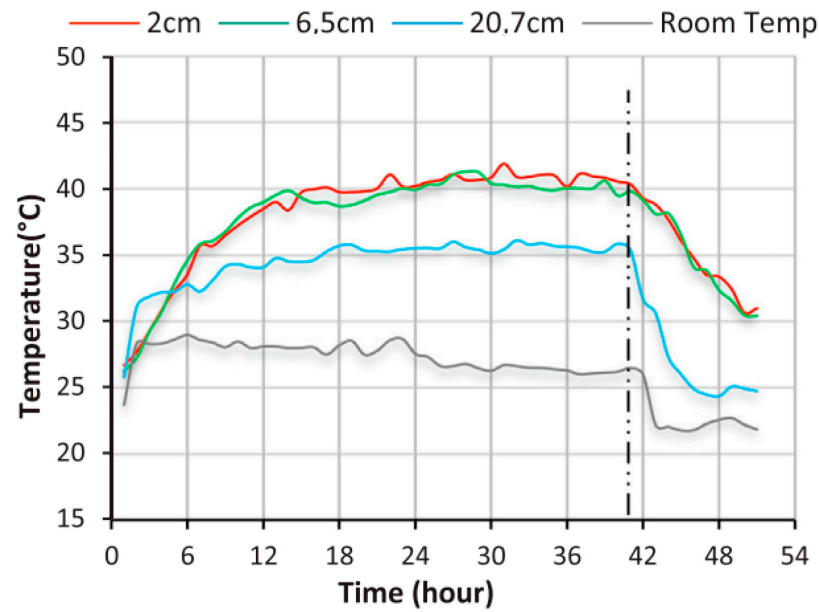


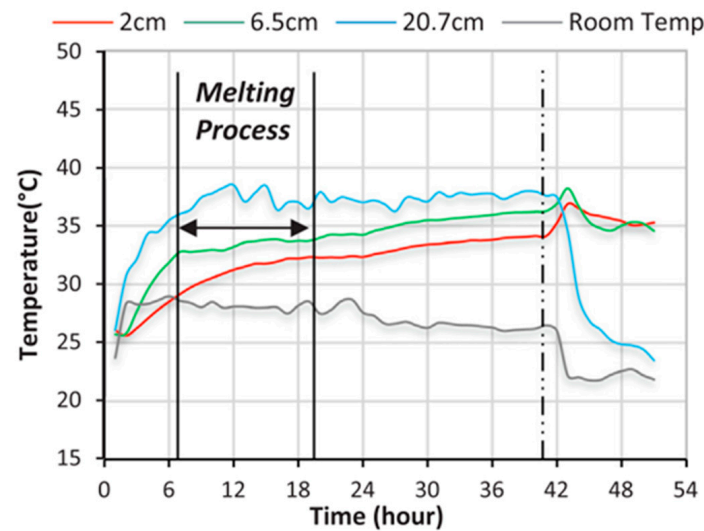
Figure 11. Evaluation of outlet water temperature of two different ponds [61].

Amirifard et al. (2018) [62] combined a solar pond with latent heat storage to improve performance stability. They analyzed three different configurations: two parallel and one series layout and presented the results in terms of temperature changes, thermal energy, and process efficiency. The conducted study evaluated the performance of four PCMs including the n-pentacosane, n-hexacosane, n-docosane and n-tetracosane. The series layout showed a 6.1% increase in average efficiency of discharging time compared to the pond without PCM, while the parallel layout showed a 5.4% increase.

Experimentally, a salt-gradient solar pond (SGSP) subjected to a solar simulator was provided for thermal evaluation by Ines et al. (2019) [63]. Environmental chambers were used for the experiments. To compare the integration and absence of ultra violet (UV) filters, two experimental prototype solar ponds were constructed in Italy. Additionally, illustrative findings demonstrating the impact of the simulator spectrum on an SGSP's temperature distribution and the consequences of thermal performance have been examined. Due to its higher potential to store latent heat, the PCM has been utilized in this study as a material that can absorb and release significant amounts of energy during solidification and melting. The outcome demonstrated that the solar pond with PCM (Plexiglas Poly (methyl methacrylate)) is capable of serving as a hot water source for home presentations by simultaneously gathering and storing solar energy. As demonstrated in Figure 12, the difference in temperature has decreased due to the pond's highest temperature being lower with PCM while the lowest temperature was roughly identical in both ponds.



(a)



(b)

Figure 12. Temperature fluctuations of SGSP without and with PCM throughout the operational time [63] (a) without phase change materials, (b) with phase change materials.

A one-dimensional model for transient heat transfer utilizing PCM was proposed by Beik et al. (2019) [64]. The convection, conduction, and radiation heat exchange with the ambient was used to determine the UCZ temperature. Paraffin Wax was utilized as PCM in the LCZ to extend the effects. According to numerical findings, a sizable amount of energy is wasted in this configuration due to reflection, walls, convection, and evaporation. Only 6% of the available solar radiation was stored, which can be improved with better insulation. Additionally, this study establishes optimal guidelines for the depth-to-radius ratio of the system, beyond which heat loss can be neglected. Moreover, the application of PCM in the solar pond yielded more stable temperatures during heat extraction, as indicated by both experimental and numerical findings.

Wang et al. (2020) [65] evaluated the effect of incorporating composite PCM heat storage capsules into the heat storage layer of a salt-gradient solar pond on its thermal

efficiency, using both numerical and experimental methods. The solar pond with PCM capsules (paraffin wax 50 and paraffin wax 60) exhibited a smaller temperature range during the phase change process compared to the conventional solar pond, but not during the non-phase transition process. Moreover, the inclusion of PCM phase change units has reduced the flow rate of the heat storage zone. The high latent heat of the PCM has a more pronounced suppressive influence on the flow. Consequently, adding PCM to the solar pond has an optimistic influence on preserving a fixed temperature and steadiness within a certain temperature range.

Rghif et al. (2021) [66] conducted a numerical investigation to determine the impact of a layer of PCM (paraffin wax) and the Dufour effect on the thermal efficiency of a salt-gradient solar pond (SGSP). The analysis considered two cases, the first case with an SGSP without a PCM layer, and the second case with an SGSP having a PCM layer located at its bottom. The findings of the simulation showed that the SGSP with a PCM layer had a lower temperature and thermal efficiency and higher heat losses across the saline water-free surface compared to the SGSP without a PCM layer. In Case 1, elevating the dimensionless Dufour coefficient from 0 to 0.8 resulted in a drop in the storage zone's dimensionless temperature from 0.894 to 0.764 and a drop in thermal storage efficacy from 37.41% to 31.85%. Similar to Case 1, Case 2 saw a reduction in the dimensionless temperature of the storage zone from 0.800 to 0.688 and a drop in the thermal storage efficacy from 33.32% to 28.66% for the same variation spectrum in the dimensionless Dufour coefficient.

A pond combined with paraffin wax PCM (RT35 HC) and a conventional one were planned, constructed, and tested by Colarossi et al. (2022) [67] to compare their respective performances. The average temperature in the pond with the RT35 HC is, according to the results, roughly 4 °C cooler over 10 days (equivalent to a 5.7% decrease). After that, a second experiment was run to compare two melting temperatures (RT35 HC and RT44 HC). According to the findings, a greater melting temperature makes it possible to smooth out temperature peaks. Due to the release of latent heat, a lower melting temperature ensures a greater and more stable temperature at night, making the application suitable in cases where a fixed temperature need at the outlet fluid is present.

In the LCZ of a small solar pond, Colarossi and Principi (2022) [68] demonstrated an innovative application of PCMs. Aluminum cylinders that have been stacked on the bottom contained paraffin wax (RT-35 HC). Both with and without the PCM, the solution's deep temperature is being tracked. With a laser shadowgraph approach, the stability of the pond is examined in order to see how thermal convection affects the surfaces. Findings indicate that after a 6 h heating cycle, the LCZ of the solar pond with PCM is approximately 3 °C cooler than the reference example. The shadowgraph study demonstrates that the reference case's increased thermal convection damages the interface to the point of failure. The solar pond is more stable, according to PCM testing.

Wang et al. (2022) [69] investigated the effect of adding steel wires to paraffin in the composite PCM on heat transfer performance. The study found that adding 10 wt% of steel wires significantly improved the heat transfer coefficient, with a greatest value of $18.17 \text{ W m}^{-2} \text{ }^{\circ}\text{C}^{-1}$ and an increase of 18.84% during melting, and a maximum value of $21.59 \text{ W m}^{-2} \text{ }^{\circ}\text{C}^{-1}$ and an increase of 20.88% during freezing. In addition, an experimental study was conducted in a solar pond with 20 PCM capsule tubes added. According to the study, the addition of RT 50 and RT 60 paraffin waxes to the solar pond reduced day-night temperature differences by 2.87 °C and 2.53 °C, respectively, compared to the conditions without any PCM. Moreover, the inclusion of RT 50 and RT 60 resulted in exergy increments of 9.34% and 14.13%, respectively. This implies that adding PCM to the solar pond improved the quality of the thermal energy produced.

In 2022, Reza et al. [70] carried out a study to compare the thermal and salinity characteristics of two pilot salt-gradient solar ponds with and without a PCM made of paraffin wax. They looked at three distinct heat extraction techniques and discovered that instability can occur at the upper and lower salinity gradient limits. The findings demonstrated that the PCM-equipped salt-gradient solar pond outperformed the pond without the PCM in

terms of average outlet temperature for the internal heat exchanger, thermal and salinity stability, and temperature drop during heat extraction. The minimum and maximum temperatures of the pond were controlled by PCM, which increased evaporation (8.4%) and enhanced thermal efficiency during rapid or prolonged heat extraction. The research additionally indicated that while heat extraction from the non-convective zone (NCZ) can affect the stability of the NCZ, heat extraction from the convective layer is preferable to that from the NCZ.

In summary, it can be stated that the maximum increase in outlet water temperature from the solar pond was 6.5% for using PCM than the case without using PCM. This is already indicated by Beik et al. (2019) [64] and demonstrated in Figure 13.

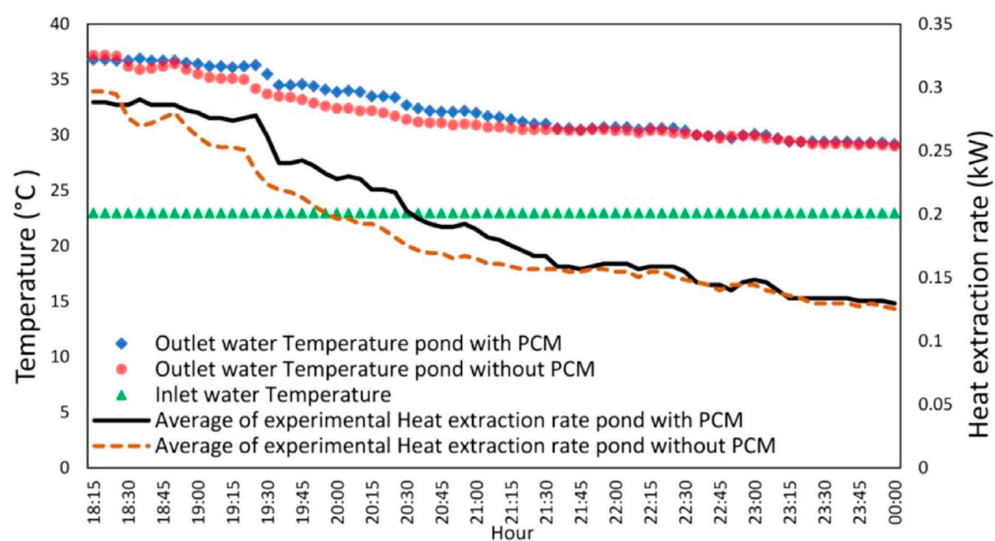


Figure 13. Heat extraction of the ponds with and without PCM and ponds’ temperature against operational time [64].

A review of the research included in Table 3 demonstrates that adding PCM units to the solar pond improved its stability and capacity to sustain a constant temperature. Moreover, utilizing the PCM in the solar pond results in a temperature that is more consistently stable while the heat is being extracted. Additionally, the average efficiency of discharging time for the series arrangement reveals a 6.1% increase in the pond without phase change material (PCM). Moreover, this increase for the parallel layout is roughly 5.4%.

2.4. Solar Air Heater-Related Studies

In order to heat air for applications such as room heating and ventilation, a solar air heater system employs solar energy. A flat plate or a group of tubes serving as the basic building blocks of a solar air heater are used to absorb sunlight and transmit heat to the air being circulated within the system. The heated air can then be utilized in place of or as an addition to conventional heating systems. The amount of sunshine available, the direction and tilt of the collector, the airflow rate, and the surrounding temperature all have an impact on how well a solar air heater performs [71]. By choosing the right collector type and size, adjusting the collectors’ orientation and tilt to maximize solar radiation, and reducing heat losses through adequate insulation, it is possible to increase the efficiency of a solar air heater system. For the system to operate at its best and last as long as possible, proper maintenance is required, including routine air filter replacement and collector cleaning [72]. In a number of applications, solar air heater systems can offer an affordable, environmentally friendly alternative for space heating and ventilation, especially in regions with ample sunlight and high heating demands.

Table 3. Outline of studies on phase change material for the solar pond.

Authors (Year) [Reference]	Configuration	Type of Study	Studied Parameters	Highlighted Results
Sarathkumar et al. (2017) [61]	Al ₂ O ₃ nanoparticles with PCM to enhance the performance of solar ponds.	Experimental	Impact of Al ₂ O ₃ with PCM in the solar pond.	Up to 7.30 p.m. in the evening, the solar pond with Al ₂ O ₃ nanoparticles was able to heat the water.
Amirifard et al. (2018) [62]	Solar pond with latent heat storage.	Experimental and numerical	Effect of using PCM.	The average efficiency of discharge time for the series arrangement is 6.1% higher in the pond without PCM. Moreover, this improvement for the parallel arrangement is roughly 5.4%.
Ines et al. (2019) [63]	Solar pond with PCM.	Experimental	Impact of PCM in the solar pond.	While the lowest temperature was roughly comparable in both ponds, the highest temperature of the pond decreased with PCM, reducing the temperature differential.
Beik et al. (2019) [64]	In the LCZ of the solar pond, paraffin wax as PCM was used.	Experimental and numerical	Effect of using PCM in the solar pond.	While extracting heat from the solar pond, using the PCM results in more consistently stable temperatures.
Wang et al. (2020) [65]	Incorporating the composite PCM heat storage capsules into the salt-gradient solar pond's heat storage layer.	Experimental and numerical	Impact of adding PCM units to the solar pond.	The solar pond's stability and ability to maintain a steady temperature were both improved with the addition of PCM units.
Rghif et al. (2021) [66]	The layer of a PCM in a salt-gradient solar pond (SGSP).	Numerical	Impact of using PCM.	In contrast to the SGSP without the PCM layer, the temperature, thermal efficiency, and amount of heat losses over the saline water-free surface are all inferior.
Colarossi et al. (2022) [67]	Solar pond integrated with PCM (RT35 HC) and a traditional one.	Experimental	Impact of PCM.	A greater melting temperature permits moderately high peaks of temperature. Yet, a lower melting point ensures a greater and steadier nighttime temperature.
Colarossi and Principi (2022) [68]	PCMs in the LCZ of a small solar pond.	Experimental	Phase change material.	After a 6 h heating cycle, the LCZ of the solar pond with PCM is approximately 3 °C cooler than the baseline example.
Wang et al. (2022) [69]	Composite PCM of paraffin and steel wires applied in the solar pond.	Experimental	Effect of PCM.	By incorporating PCM, solar ponds can produce heat that is of higher quality and with a wider range of applications.
Reza et al. (2022) [70]	Using Paraffin Wax (PW) as the phase transition material in two pilot salt-gradient solar ponds and not in them (PCM).	Experimental and analytical	Effect of PCM.	Higher evaporation (8.4%) in the SPP was caused by the use of PCM to regulate the maximum and minimum temperatures of the pond.

There are profound advantages and a few limitations and shortcomings of the current utilization of PCMs as thermal energy storage in solar air heaters. This section covers a broad range of topics related to PCMs, including their thermal properties, applications, and challenges.

Research on the thermal efficiency of a v-corrugated plate solar air heater and a flat plate solar air heater with and without PCM (paraffin wax) at various mass flow rates of 0.062, 0.028, and 0.009 kg/s was undertaken by Kabeel et al. (2016) [73]. They also looked into the impact of changing the PCM's thickness beneath the absorber plate. According to the experimental results, the flat plate solar air heater with the same mass flow rate of 0.062 kg/s had a temperature of 1–5.5 °C for 2.5 h after sunset while the v-corrugated plate solar air heater's outlet temperature was 1.5–7.2 °C greater than the surrounding temperature when PCM was used. Furthermore, the outcomes presented in Figure 14 indicate that the v-corrugated plate solar air heater equipped with PCM had a 12% higher daily performance than the one without PCM. Moreover, when the mass flow rate was 0.062 kg/s, the v-corrugated plate solar air heater with PCM showed a 15% and 21.3% improvement in daily performance compared to the flat plate solar air heater with and without PCM, respectively.

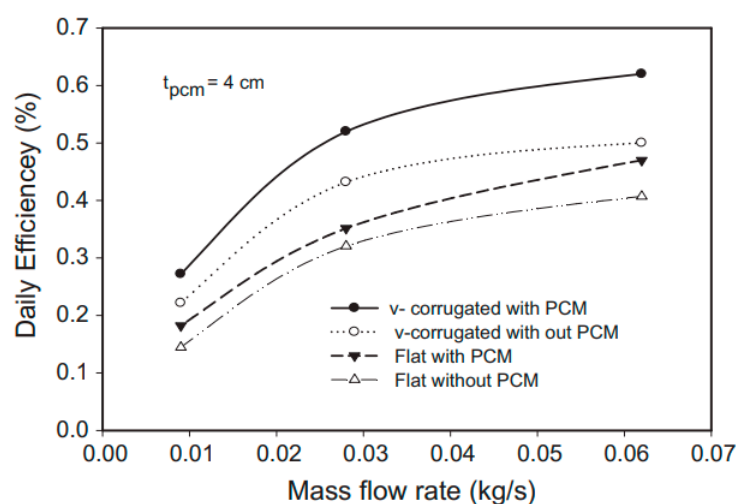


Figure 14. An assessment of daily performance between v-corrugated and flat plate solar air heaters vs. the mass flow rates with and without PCM [73].

El Khadraoui et al. (2017) [74] developed an indirect forced convection solar dryer using PCM (paraffin wax). A solar air panel heats the drying agent directly, while a drying chamber and a solar energy accumulator (a solar air collector with a PCM cavity) are also part of the system. The objective of this study was to investigate the feasibility of using a solar air heater with PCM to store solar energy during the day and release it at night. The solar dryer was tested both with and without PCM while under no load. The solar energy accumulator's daily energy effectiveness was estimated to be 33.9%, compared to its daily energy efficiency of 8.5%. The findings show that after employing the solar energy accumulator, the drying chamber's temperature stayed 4–16 °C above the surrounding air throughout the night. Moreover, when using the solar dryer with PCM, the relative humidity in the drying chamber was 17–34.5% lower than the ambient relative humidity.

A double-pass solar air heater was studied by Salih et al. (2019) [75] using a series of rectangular capsules filled with PCM made of paraffin wax. The innovative system was tested during the charge/discharge process using an indoor projector simulator, and the three-dimensional forced convection turbulent flow in the double-pass solar heater was solved using a model based on a SIMPLE solver. As shown in Figure 15, the results revealed that raising the air flow rate caused the melting duration to take longer and the paraffin melting temperature to drop. For different sun intensities of 825 W/m², 725 W/m²,

and 625 W/m^2 at the same airflow speed of 0.6 kg/min , it was discovered that the heater's best discharging period and air temperature increase were 3 h with $17.95\text{--}3 \text{ }^\circ\text{C}$, 2 h with $14\text{--}3 \text{ }^\circ\text{C}$, and 1.25 h with $11\text{--}2.5 \text{ }^\circ\text{C}$.

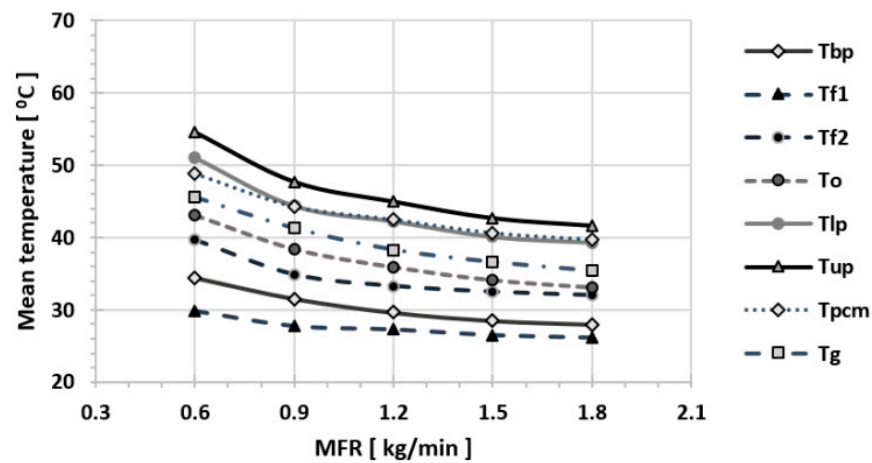


Figure 15. The mean temperature in the DP-SAH with PCM versus air MFR for various solar irradiance of 825 W/m^2 [75].

The thermal efficiency of solar air heaters was studied in experiments by Abuşka et al. (2019) [76] to determine the effects of employing PCM and honeycomb as an internal fin structure in the PCM panel. A total of 6 different air mass flow rates, ranging from 0.008 to 0.048 kg/s , were used during the tests. A total of 2 distinct configurations of the heat storage material were tested. The Type I heater (which utilized PCM with a honeycomb core) and the Type II heater (which used solely PCM). The third heater (Type III), which served as a reference, had a flat absorber plate without PCM. The findings revealed that for mass flow rates of 0.032 , 0.04 , and 0.048 kg/s , the Type I and II heaters with PCM's average daytime thermal performance improved from 8.4% to 9.0% , while for mass flow rates of 0.008 , 0.016 , and 0.024 kg/s , it declined from 0.8% to 8.0% . The heater without honeycomb was more effective by 0.1% to 4.4% per day when compared to the heaters with PCM, according to the comparison. The Type I and II heaters with PCM were more effective, ranging from 2.6% to 22.3% , when the daily thermal performance was taken into account, especially at high mass flow rates.

The study conducted by Raj et al. (2019) [77] aimed to improve the thermal efficiency of the double-pass solar air heater system (DPSAHS) by incorporating PCM with thermal lag. Additionally, they investigated the impact of metallic macro-encapsulation on the heat storage and recovery of the PCM coupled with the DPSAHS. The study investigates the impact of encapsulation geometry on the storage and discharge of organic paraffin wax PCM. The research found that rectangular and cylindrical macro-encapsulates equipped with DPSAHS had an average encapsulation performance of 47.2% and 67% , respectively. The study also compared the performance of DPSAHS with and without PCM storage. The analysis showed that the DPSAHS with PCM storage improved operational time at a slightly higher construction cost.

SunilRaj et al. (2020) [78] conducted an experiment on a solar air heater with a V-trough solar thermal collector integrated with PCM (paraffin wax) blended with Al_2O_3 nanomaterials at a fill ratio of 0.90 , and a drying chamber. The experiment aimed to test the efficiency of the system in drying 0.5 kg capsicum, and the results demonstrated a significant enhancement in moisture removal. The researchers determined that the design of the system is uncomplicated and exhibits excellent thermal efficiency. The research was carried out under sunny conditions in Bengaluru (12.96° N , 77.63° E) and demonstrated that the daily thermal efficiency of the air heater with thermal storage system ranged from 12% to 65% .

In order to assess the temperature responsiveness and competence of a standard solar air heater (SAH) with SAH fitted with a PCM constructed of paraffin packs, Ameri et al. (2021) [79] conducted an experiment. The experiment looked at how the use of PCM, its melting temperature, and the layout of slabs of PCM with various melting points affected the thermal responsiveness of SAHs. On a Board, four distinct combinations of 2 kinds of paraffin wax with various melting temperatures between 40 °C and 50 °C were fitted. In Kerman, Iran, the experiment was carried out at two separate air mass flow rates. The findings demonstrated that utilizing PCM increased the SAH's daily thermal efficiency from 53.1% to 62.6%. Using PCM with a greater melting point temperature, SAHs' outlet temperatures rose by over 5 °C, and their daily efficiency increased by approximately 3%. (Figure 16). The experiment also showed that the configuration with evenly distributed PCM types with various melting points had the best daily thermal efficiency and produced an enhanced thermal efficiency of approximately 5%.

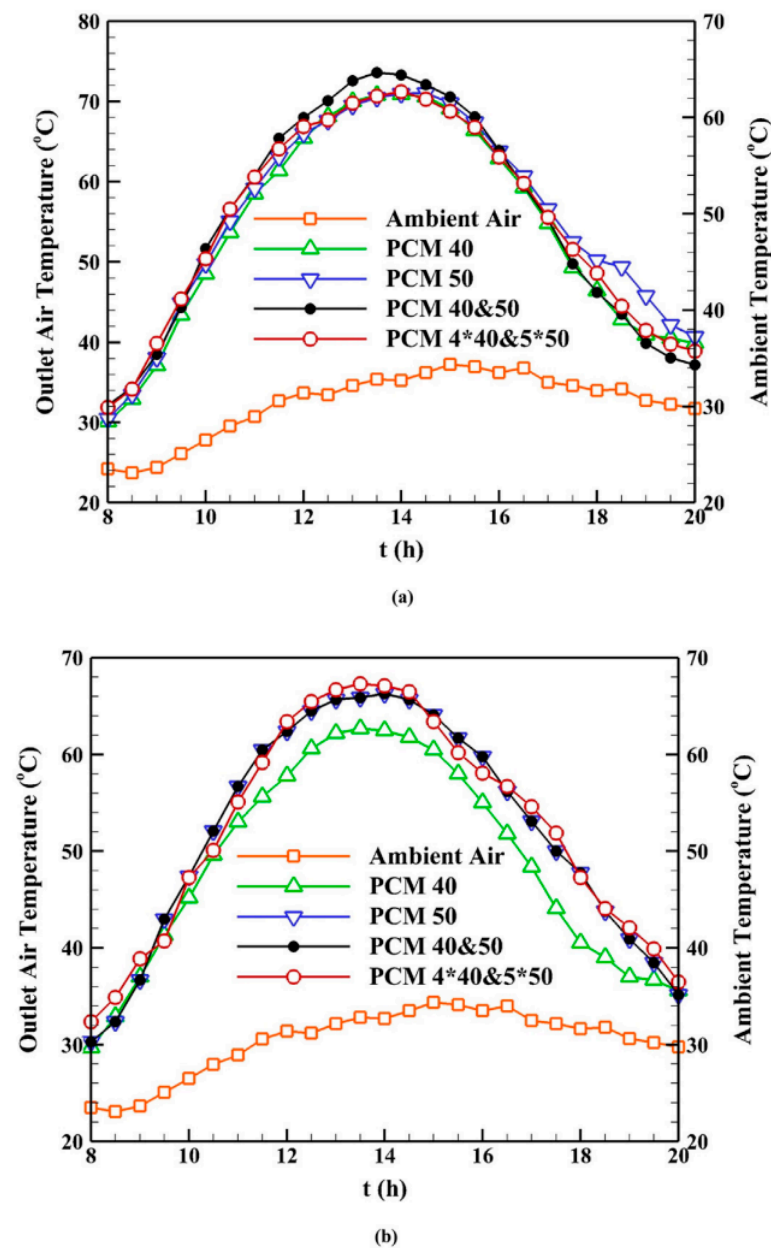


Figure 16. The variation of outlet temperatures in different scenarios for air mass flow rates of (a) 0.006 kg/s and (b) 0.01 kg/s, data acquired on 20 July 2019, and 21 July 2019 [79].

Mahdi and colleagues (2021) conducted numerical simulations to investigate the melting/solidification process in a metal foam containing PCM for both sequential and simultaneous operational modes. Specifically, Mahdi et al. (2021) [80] used organic phase change material paraffin wax type RT70HC (RUBITHERM). The composite was included in a rectangular compound that heated a room as a space heater after being cooled by air flowing through a central channel. As a result of quicker charging rates than mode II, the results showed that modes I (8 h charging and 8 h discharging separately) and III (2 h charge and 14 h simultaneous charging-discharging) both reached full melting (2 h charging and 2 h discharging separately, repeated for 16 h). The temperature distribution in Mode III was more uniform, leading in consistent heat transfer between the PCM and cooling fluid. Increasing the porosity of the metal foam had a negative impact on the rate of liquid development, resulting in complete PCM melting in 6.5 h for 90% porosity and 78% melting in 8 h for 95% porosity. Moreover, by increasing the air flow rate from 0.01 kg/s to 0.03 kg/s, the final mean temperature of the PCM was reduced from 69.9 °C to 66.4 °C.

Madhulatha et al. (2021) [81] utilized ANSYS FLUENT to optimize TESS design through numerical analysis. The researchers evaluated three diverse PCMs, including paraffin wax, n-octadecane, and calcium chloride hexahydrate ($\text{CaCl}_2 \cdot 6\text{H}_2\text{O}$), and examined inline, staggered, and circular arrangements of tubes in the TESS. They altered the air intake temperature to TESS from 40 °C to 125 °C and adjusted the mass flow rate of air velocity at the inlet from 3.5 to 5.5 m s^{-1} in steps of 0.5 m s^{-1} . The results introduced the average tube wall temperature, average surface heat transfer coefficient, average PCM temperature in tubes, and average heat absorbed by PCM. When comparing staggered and inline grid arrangements, tubes in staggered arrangements were found to increase heat absorbed by PCM by 10.45% and 48.03%, respectively, with paraffin wax and $\text{CaCl}_2 \cdot 6\text{H}_2\text{O}$ as PCMs, while there was an insignificant 0.09% improvement with n-octadecane.

Dinesh et al. (2022) [82] carried out a study to test the efficacy of a baffled solar-based air heater (SAH-BP) with organic PCM backup. The investigation was carried out over two similar solar days in February 2021 and interacted with operating modes, namely baffled SAH without organic PCM (SAH-BP) and baffled SAH with organic PCM. The organic PCM was stored underneath the absorber, and the baffle plates were connected over the absorber surface in an alternate sequential manner. The trials were kept at a constant flow rate of 0.18 kg/s and the organic PCM utilized was regular commercial-grade paraffin. The findings demonstrated that the baffled SAH's energy efficiency was increased by 11.25% by adding organic PCM.

The energy consumption (EC) of a conference hall in Riyadh that had a timetable of occupancy from 8 a.m. to 12 p.m. was evaluated by Abu-Hamdeh et al. in 2022 [83]. The installation of an economizer and heat recovery equipment allowed for the development of software that changes the active and inactive hours in accordance with the mechanical ventilation timetable. In the first method, the injection of cold air into the indoor area in the summer was adjusted in the range of 3–12 (i.e., ACH = 3, 6, 9 and 12) by constructing programming on the air change (ACH) parameter. The findings showed that the economizer's effectiveness was more apparent with a lower ACH value. The economizer's performance was lower than expected, despite the improvement in ACH, leading to a maximum decrease of 3.07% in EC. In the second method, a program was developed to limit the use of heat recovery to the temperature difference between the interior and exterior of the building. By using this method, EC was decreased by 34% in the summer and 95% in the winter. Yet, the yearly EC drop was capped at 35% because of the significant amount of cooling load. In the third procedure, HS29 PCM was introduced to the structure, and it was found that while it occasionally performed poorly during the winter, it performed admirably throughout the summer. The approach utilized has ultimately decreased annual EC by 5.6%.

An experiment was carried out by Palacio and colleagues (2022) [84] to investigate the effectiveness of a double-channel solar air heater (SAH) with and without a PCM used as a thermal energy storage system. In order to include macro-encapsulated PCM

(Rubitherm RT 45) in the absorber plate, one of two similar prototypes was adjusted. The three weather conditions that were tested in the study were clear skies with strong solar radiation, partly cloudy skies, and clear skies with a large decrease in solar radiation at noon. The experiment demonstrated that the double-channel solar air heater (SAH) with a PCM as a thermal energy storage system had maximum outlet temperatures of 82 °C, 62 °C, and 79.5 °C for the three cases studied, respectively. In contrast, the SAH without PCM consistently had an outlet temperature that was 10 °C lower than the SAH with PCM. The PCM enabled the system to maintain heating during day irradiation transients and extend it after dusk without affecting thermal efficiency.

Chaatouf et al. (2022) [85] conducted a study on a solar air heater (SAH) integrated with a PCM storage unit to optimize its efficiency for drying apricots. The SAH was analyzed under real meteorological conditions in Eastern Morocco using the computational fluid dynamics (CFD) method and a C++ UDF (User-Defined Function) subroutine written in the C++ programming language ((Note: C++ UDF is a type of function used in CFD, such as ANSYS Fluent, to extend the functionality of the software beyond the built-in capabilities). To meet the drying needs of apricots, the SAH was subjected to testing with natural and forced convection and optimization based on different tilts and air velocities. Results showed that without PCM, the SAH produced high temperatures above 70 °C that could negatively affect product quality. However, with a PCM layer (paraffin RT RT58), the temperature decreased throughout the day and increased after sunset, with an optimal combination of 1 m/s air velocity and 4 cm PCM thickness for forced convection. For natural convection, a 60° tilt was found to be appropriate for enhancing the mass flow rate, which significantly affected the outlet temperature of SAH and the melting process of PCM. In the drying chamber, these two ideal instances were further examined.

Verma et al. (2022) [86] used a transient computational iterative solution procedure to predict the thermal efficiency of a solar air heater with PCM (paraffin wax RT42) using differential airflow arrangements. The finite volume method was employed to solve the governing differential equations. The researchers used the first-order upwind advection scheme to stimulate air temperatures. The findings demonstrated that the PCM integrated into the solar air heater enabled large thermal energy storage, instantaneous and prolonged thermal backups, and air heat gain as corresponding to the daytime and changeable air flow rate configurations. The highest thermal performance was 63% at 0.05 kg/s total mass flow rate. The airflow rate settings that can deliver an outlet air temperature of at least 303 K during the night were also found by the researchers.

Sharol et al. (2022) [87] conducted an experimental analysis to investigate the effect of incorporating a thermal energy storage material inside the tube of a double-pass solar air heater with a cross-matrix absorber (DPSAH-CMA) on its thermal efficiency. The researchers tested the SAH under different operating conditions both indoors and outdoors. Results showed that the DPSAH-CMA with PCM (paraffin wax) was able to buffer thermal energy more effectively, with a rate of $-0.81 \text{ }^\circ\text{C min}^{-1}$, compared to the one without PCM at a mass flow rate of 0.005 kg/s. The PCM also led to an increase in the cumulative heat rate of the DPSAH-CMA, with an extreme value of 1548.54 W at the greatest solar radiation of 900 W m^{-2} . The maximum storage performance of the DPSAH-CMA with PCM was at the matching greatest mass flow rate and was inversely related to solar radiation values. When comparing the performance of the two SAHs under outdoor conditions, the DPSAH-CMA with PCM attained the greatest thermal performance, outperforming the DPSAH-CMA without PCM by 17%. Moreover, the DPSAH-CMA's exergy efficiency was found to be 23% with PCM and 15% without PCM, as per Sharol et al. (2022) [87].

Unidirectional flow, PCM-rod (ZN-110H), and spiral tubes were used in an experiment by Luo et al. (2002) [88] to increase the thermal performance of an evacuated tube solar air heater. Using an experimental test platform, the thermal efficiency of the SAH-PCM was assessed. ANSYS software was utilized to examine the temperature and flow fields in the vacuum tube, and an environmental assessment was performed. The numerical study identified the ideal PCM-rod size and estimated the spiral tube's heat augmentation

coefficient to be 1.1. The results of the experimental testing showed that the SAH-PCM could effectively prevent outlet temperature swings, albeit at the expense of a 31.5 °C lower average outlet temperature. The rate of heat loss was decreased by 58.5%, and PCM's thermal efficiency could increase to 844.9%. Moreover, the operation hours at night were extended by over 3 h. These findings demonstrate that phase change materials and spiral tubes, as well as unidirectional flow structural design, can enhance the thermal efficiency of the air heater.

Farzan et al. (2022) [89] developed a double-pass solar air heater with a perforated absorber plate and integrated PCM. Three scenarios were tested over 24 h at two mass flow rates. Results showed the use of PCM and PCM/EMM increased total heat gain and energy efficiency by approximately 45.88% and 48.19%, respectively, compared to traditional SAHs. The SAH with PCM/EMM had a higher exhaust temperature in the evening, reaching 76% daily performance, but reduced exergy efficiency due to lower exhaust air temperature.

A form of construction material that uses PCMs in a ventilation system to control indoor temperatures and save energy is known as an interlayer ventilated phase change material (IVPC) system was developed in 2023 by Fan et al. [90] (Figure 17). A layer of PCM is often sandwiched between two layers of construction material, such as drywall or plasterboard. A ventilation system is subsequently built underneath the PCM layer, and the PCM layer is perforated to facilitate airflow. The PCM layer becomes heated by solar light during the day, melting and absorbing heat. The PCM solidifies at night when the temperature decreases and releases heat. Air is circulated through the perforations by the ventilation system behind the PCM layer, which enables the heat to be dispersed uniformly throughout the structure. This facilitates temperature control indoors and lessens the demand for HVAC systems. Buildings with a lot of thermal mass, such as concrete or masonry structures, benefit greatly from interlayer ventilated PCM systems. Utilizing PCMs can increase the thermal mass of the building, enhancing its capacity to absorb and store heat. The ventilation system also aids in keeping the PCM layer from overheating and keeps the building's temperature constant [90].

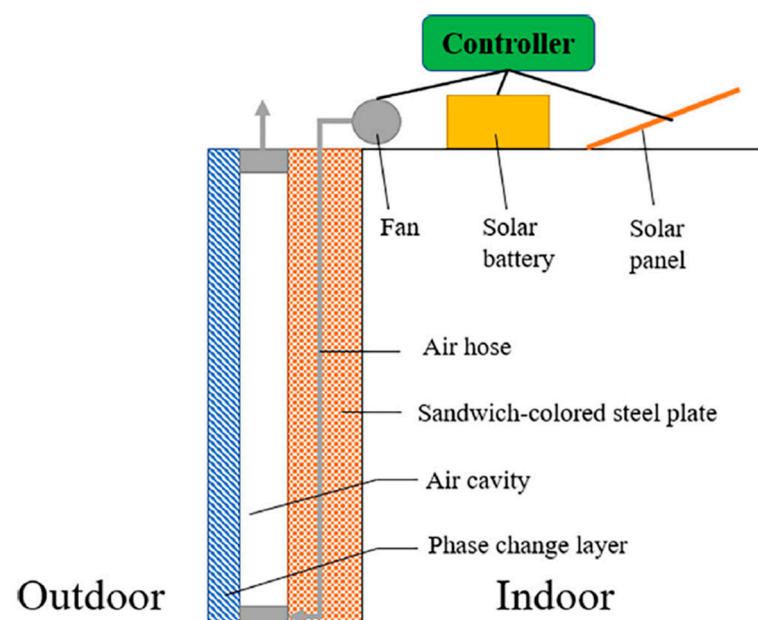


Figure 17. The basic structure of an interlayer ventilated phase change material [90].

Interlayer ventilated phase change material (IVPC), which can be used in conjunction with a solar air collector to boost thermal performance, was proposed by He et al. (2022) [91]. The performance of the IVPCs (PCM24 and EGPCM) was evaluated by trials, and the findings indicated that the ideal solar hot air supply temperature and speed should be between 35 and 45 °C and 3 to 4 m/s, respectively, when the IVPC finished the latent heat

storage process. Five hours could pass while the latent heat release time was preserved. The impact of linking the IVPC with a solar air collection system (IVPSS) on heating temperature changes in a rural building located in a cold region of China was also simulated by the researchers using TRNSYS (Transient System Simulation Tool). TRNSYS is a software package for simulating the behavior of energy systems. In comparison to buildings without the IVPSS, the IVPSS was able to keep the inside temperature of the building within the range of 8 to 16 °C, a rise of 5 to 8 °C. This shows that the IVPC can efficiently utilize solar energy to change peak loads, decrease temperature swings in rooms, and enhance indoor thermal comfort, offering a clean energy alternative for heating farms in cold climates.

Brahma et al. (2023) [92] deliberate a new solar air heater (SAH) with the ability to incorporate PCM at the Department of Energy, Tezpur University. The performance of a solar air heater (SAH) integrated with different PCMs, namely acetamide, stearic acid, and paraffin wax, was evaluated and compared with a conventional SAH during both charging and discharging periods. The absorbed, useful, and lost heat were estimated for all three PCMs, and it was observed that paraffin wax exhibited the highest values for absorbed heat (36.56 kW), useful heat (14.13 kW), stored heat (21.59 kW), and efficiency (52.83%). Stearic acid (52.31%) followed closely behind, while acetamide (47.25%) had the lowest efficiency. The performance of the SAH with acetamide was indicated to be 15.09% higher than that of the SAH without acetamide, while the efficiency of the SAH with paraffin wax was 8.18% higher than that of the SAH without PCM, and the performance of the SAH with acetamide was 6.67% higher than that of the SAH without PCM.

A recent study by SunilRaj and Eswaramoorthy (2023) [93] evaluated the performance of a forced convection V-trough solar air heater (FCVTSAH) that incorporated a latent thermal energy storage system. The FCVTSAH system included a three-pass solar air heater, an absorber unit containing paraffin wax as a phase change material, an air blower, and a cylindrical drying unit. The authors used dry air temperatures ranging from 35 °C to 68 °C to assess the FCVTSAH's thermodynamic capability for drying agricultural items. The experimental tests were conducted at coordinates (12.96° N and 77.63° E) from 20 April to 22 April, 2020. The study reported that the energy performance of the FCVTSAH ranged from 2% to 50.5% on average, while its exergy performance ranged from 2.4% to 25%. The energy and exergy efficiencies of the latent heat storage unit were between 20.3% and 24.5% and 8.9% and 12.8%, respectively. Additionally, the drying unit's energy efficiency ranged from 20.5% to 74.3%.

A list of studies on phase change material for solar air heaters is shown in Table 4. The analysis of the trials in Table 4 can demonstrate that the storage efficiency of DPSAH-CMA with PCM was proportionate to solar radiation values and was optimum at higher mass flow rates. On a daily basis, the air heater's thermodynamic performance varies between 12% and 65% when equipped with a thermal storage system. When using PCM such as paraffin wax, n-octadecane, and $\text{CaCl}_2 \cdot 6\text{H}_2\text{O}$ and tubes arranged in a circular pattern, heat absorption by the PCM was enhanced by 9.17%, 1.55%, and 1.08%, respectively, compared to tubes in a staggered design.

Table 4. Outline of studies on phase change material for solar air heater.

Authors (Year) [Reference]	Configuration	Type of Study	Studied Parameters	Highlighted Results
Kabeel et al. (2016) [73]	Varying the thickness of PCM below the absorber plate.	Experimental	Altering the thickness of PCM underneath the absorber plate and its impact.	The outlet temperature of the v-corrugated plate solar air heater with PCM was higher than that of the flat plate solar air heater, ranging from 1.5–7.2 °C above ambient air temperature during the 3.5 h after sunset, compared to 1–5.5 °C for the flat plate solar air heater with a mass flow rate of 0.062 kg/s.
El Khadraoui et al. (2017) [74]	Solar dryer using PCM.	Experimental	Impact of PCM in SAH.	It was discovered that the relative humidity in the drying chamber of the solar dryer with PCM was 17 to 34.5% lower than the relative humidity in the immediate vicinity.
Salih et al. (2019) [75]	Double-pass solar air heater using multiple rectangular capsules filled with paraffin wax based on a PCM.	Experimental and numerical	Air flow rate and PCM.	The increased airflow rate causes the melting process to take longer to complete and lowers the paraffin’s melting temperature.
Abuşka et al. (2019) [76]	The PCM panel of SAH utilizes honeycomb as the internal fin structure along with PCM.	Experimental	Impact of PCM and honeycomb.	At mass flow rates of 0.032, 0.04, and 0.048 kg/s, the Type I-II heaters showed an average daytime thermal performance increase from 8.4% to 9.0%. Conversely, at mass flow rates of 0.008, 0.016, and 0.024 kg/s, the average daytime thermal performance decreased from 0.8% to 8.0%.
Raj et al. (2019) [77]	Double-pass solar air heater system with PCM.	Experimental	The effect of the geometry of encapsulation used for storage.	For DPSAHS fitted with rectangular and cylindrical macro-encapsulates, average encapsulate efficiencies of 47.2% and 67%, respectively, were found.
SunilRaj et al. (2020) [78]	PCMs mixed Al ₂ O ₃ nanomaterials are inserted in a V-shaped solar thermal collector that makes up the SAH.	Experimental	Thermal energy storage.	The daily thermal efficiency range of an air heater with thermal storage system is 12% to 65%.
Ameri et al. (2021) [79]	The traditional solar air heater and the solar air heater with paraffin phase change material (PCM).	Experimental	Using PCMs in SAHs.	The output temperature of SAHs increases by nearly 5 °C when PCMs with higher melting point temperatures are used, and the daily performance of SAHs decreases by approximately 3%.

Table 4. Cont.

Authors (Year) [Reference]	Configuration	Type of Study	Studied Parameters	Highlighted Results
Mahdi et al. (2021) [80]	SAH with metal foam saturated with PCM.	Numerical	The effect of the metal foam and the variation in coolant flow rate on the solidification performance.	The porosity and liquid development rate are negatively related. When the air flow rate is increased from 0.01 kg/s to 0.03 kg/s, the end means PCM temperature decreased from 69.9 °C to 66.4 °C.
Madhulatha et al. (2021) [81]	The SAH was evaluated using three distinct PCMs, namely paraffin wax, n-octadecane, and calcium chloride hexahydrate (CaCl ₂ ·6H ₂ O).	Numerical	Type and arrangement of PCM.	When using paraffin wax, n-octadecane, and CaCl ₂ ·6H ₂ O as the PCM, tubes in a circular layout boosted PCM's ability to absorb heat by 9.17%, 1.55%, and 1.08%, respectively, relative to tubes in a staggered design.
Dinesh et al. (2022) [82]	Baffled solar-based air heater with organic PCM.	Experimental	Impact of organic PCM in a baffled SAH.	The integration of organic PCM into the confused SAH improved its energy-efficiency performance.
Abu-Hamdeh et al. (2022) [83]	Solar air heater equipped with PCM.	Experimental	Impact of using PCM.	The solar air heater's yearly EC was eventually decreased by 5.6% by using PCM.
Palacio et al. (2022) [84]	Double-channel solar air heater (SAH) with and without PCM.	Experimental	PCM in the SAH.	The SAH with PCM's highest outlet temperatures in the three cases were, respectively, 62 °C, 82 °C, and 79.5 °C.
Chaatouf et al. (2022) [85]	SAH with a heat storage unit made of PCM block.	Numerical	The SAH's performance can be affected by the type of PCM used and its thickness.	The temperature is changed by adding a PCM layer so that it drops during the day and rises at night.
Verma et al. (2022) [86]	PCM embedded parallel flow in solar air heater.	Numerical	Impact of PCM embedded parallel flow in solar air heater.	With a total mass flow rate of 0.05 kg/s, the highest heat efficiency of roughly 63% is attained.

Table 4. Cont.

Authors (Year) [Reference]	Configuration	Type of Study	Studied Parameters	Highlighted Results
Sharol et al. (2022) [87]	A double-pass solar air heater with a cross-matrix absorber and thermal energy storage material inside the tube.	Experimental	The impact of incorporating a thermal energy storage material inside the tube of a double-pass solar air heater.	The greatest DPSAH-CMA-with-PCM storage efficiency was achieved at greater mass flow rates and was inversely correlated with solar radiation levels.
Luo et al. (2002) [88]	A solar air heater with evacuated tubes, featuring unidirectional flow, a PCM-rod, and a spiral tube.	Experimental	The structural design, spiral tube, and the use of PCM.	The use of phase change materials, spiral tubes, and unidirectional flow in the air heater’s structural design can enhance its thermal performance.
Farzan et al. (2022) [89]	Novel double-pass SAH design using integrated PCM and a perforated absorber plate.	Experimental	Effect of PCM/EMM.	The innovative SAH employing PCM/EMM has a daily efficiency of 76%.
He et al. (2022) [91]	An interlayer ventilated PCM component coupled with SAH.	Experimental and numerical	Impact of PCM coupled with SAH.	The ideal solar hot air supply temperature and speed are 35–45 °C and 3–4 m/s, respectively, if IVPC successfully stores latent heat.
Brahma et al. (2023) [92]	Novel solar air heater with the provision of integrating PCM.	Analytical	Impact of using acetamide in SAH.	It was discovered that SAH with acetamide was 15.09% more effective than SAH without acetamide; likewise, SAH with paraffin wax was revealed to be 8.18% more effective; and acetamide was discovered to be 6.67% more effective than SAH without PCM.
SunilRaj and Eswaramoorthy (2023) [93]	V-trough solar air heater with latent thermal energy storage unit.	Experimental	Effect of latent thermal energy storage unit.	Latent heat storage units’ respective energy and exergy efficiencies range from 20.3% to 24.5% and 8.9% to 12.8%.

The following Equation (1) represents the thermal energy balance required to characterize the operation of solar air collectors [94]:

$$M_C C_P \frac{dT_{p,ave}}{dT} + m C_P (T_{out} - T_{in}) = \eta_0 I A_C - U_C (T_{p,ave} - T_e) A_C \quad (1)$$

M_C is the mass of the collector, m is the mass flow rate, C_P is air-specific heat, $T_{p,ave}$ is the average plate temperature, T is the temperature, T_{out} , T_{in} are outlet and inlet temperatures, respectively, η_0 is the optical yield, I is the solar radiation, A_C is the surface area of the collector, U_C is the energy loss coefficient, and finally T_e is the temperature of the environment. The energy loss coefficient takes into account all collector losses, including those at the top, sides, and bottom. Temperature and emissivity of the absorbent bed, as well as wind convection on the top cover, have a significantly bigger impact on these losses than any other element.

2.5. Solar Chimney-Related Studies

A solar chimney system is a piece of equipment that powers natural ventilation in buildings using solar power. A solar chimney's fundamental structure is composed of a tall, vertical shaft with a glass surface that lets light in to warm the air inside. Vents are situated at the base of the chimney, and when the air inside the chimney warms up, it rises and pulls cooler air in. A flow of air produced by this natural convection can be utilized to cool and ventilate the building [95]. A solar chimney's efficiency is affected by a number of variables, such as the chimney's height and direction, the size and location of the vents, and the amount of solar radiation available. A solar chimney system's effectiveness can be increased by using high-quality building materials, choosing the right chimney shape and size, and orienting and positioning the chimney to catch as many sun rays as possible. For the system to operate at its best and last as long as possible, proper maintenance is required, including cleaning the vents and checking the efficiency of the chimney [96]. Notably in hot and dry locations, solar chimney systems can offer an affordable, environmentally friendly alternative for natural ventilation and cooling in buildings.

The current section presents a comprehensive review of existing research on PCMs on the solar chimney providing a critical analysis of the findings and discussing potential limitations or gaps in the research.

Li et al. (2017) [97] developed a numerical model to investigate the influence of different parameters on the thermal efficiency of a solar chimney coupled to PCM (paraffin RT 42). The model was validated, and the parameters studied included air flow rate, melting/freezing time, and temperature difference between the inlet and outlet. The study found that the phase change temperature of the PCM had a significant impact on the thermal efficiency of the solar chimney, with wider phase change temperature differences leading to earlier complete melting. However, this also caused fluctuations in room air temperature, which may result in thermal discomfort. The specific heat of the PCM affected the contribution of sensible heat to the melting/freezing process. The research findings indicate that enhancing the thermal conductivity of the PCM resulted in a rise in the air temperature difference and average mass flow rate from 1.5 to 2 °C, and from 0.033 to 0.038 kg/s, respectively, as the thermal conductivity increased from 0.2 to 0.6 W/m °C.

Bin et al. (2017) [98] investigated the impact of PCM position in the hybrid wall on the chimney effect, temperature, air velocity, and mass flow rate. As shown in Figure 18, a greater temperature difference was observed between the heating surface and the air gap than between PCM and the absorber. The conductivity of $\text{Na}_2\text{CO}_3 \cdot 10\text{H}_2\text{O}$ PCM and chimney effect during charging time caused convection that led to an immediate increase in the heat surface temperature of PCM, followed by a brief period of fixed temperature (melting temperature) if the density of radiating heat was sufficient. However, in the absence of steady temperature, the heat surface temperature of PCM declined rapidly during the discharging time (solidification temperature).

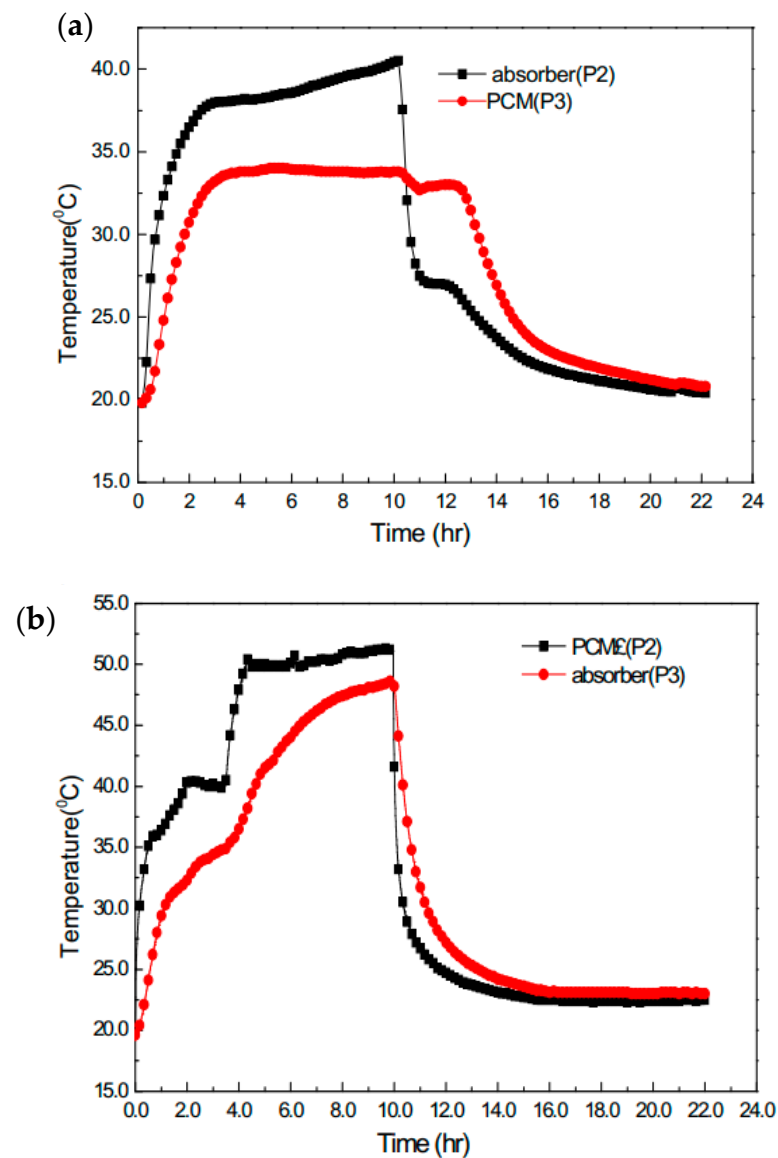


Figure 18. The heated surface temperature development of PCM and absorber [98]. (a) the heated surface temperature development of PCM and absorber when PCM was behind of the absorber at the height of 750 mm, (b) the heated surface temperature development of PCM and absorber when PCM was in front of the absorber at the height of 750 mm.

In order to improve natural ventilation and decrease heat gain admittance, Thantong et al. (2018) [99] published an evaluation of the thermal performance of a new arrangement of solar chimneys incorporating a phase change material (SC-PCM) (RT 42 paraffin wax). A 0.05 m air gap separates the two walls of this SC-PCM, which is made up of two walls. Three layers make up the exterior wall that faces the sun; the first is a cement board panel that has been painted black and is only 0.01 m thick. A paraffin-containing tank (0.015 m × 0.8 m × 1.28 m) is the second stratum. A 0.005 m thick zinc sheet makes up the third layer. The inner wall is made of thin, 0.07 m thick concrete. The SC-PCM was incorporated into the south facade of a modest house with a volume of 4.05 m³ and walls that were 10 cm thick from concrete. Another home model with the same volume was used to contrast thermal efficiencies to a straightforward concrete wall (SW). Figure 19 illustrates the experimental findings that the interior temperature of the solar chimney with PCM room was lower than that of the room with a single concrete wall.

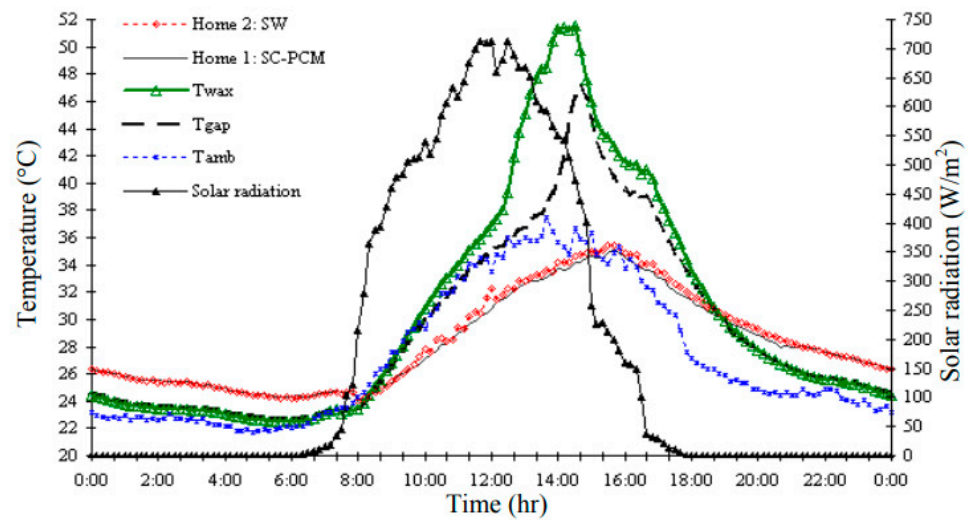


Figure 19. Hourly change in temperature of indoor air of the two houses, wax and air gap of the SC-PCM, ambient temperature and solar radiation on the vertical plane (5 February 2017) [99].

In their 2018 study, Fadaei et al. investigated the impact of latent heat storage (LHS) on a solar chimney pilot, conducting two sets of experiments—one with paraffin wax (C20) PCM and one without. Using a 3 m chimney height and 3 m collector diameter on the University of Tehran campus, they measured temperature and velocity parameters to evaluate the system’s efficiency. Results showed that the maximum air velocity was 2 m/s for the system with PCM thermal storage, compared to 1.9 m/s for the conventional solar chimney. The maximum absorber surface temperature was also 3 °C higher for the PCM system than the conventional system. The LHS system increased the average mass flow rate of the pilot by approximately 8.33%, as shown in Figure 20.

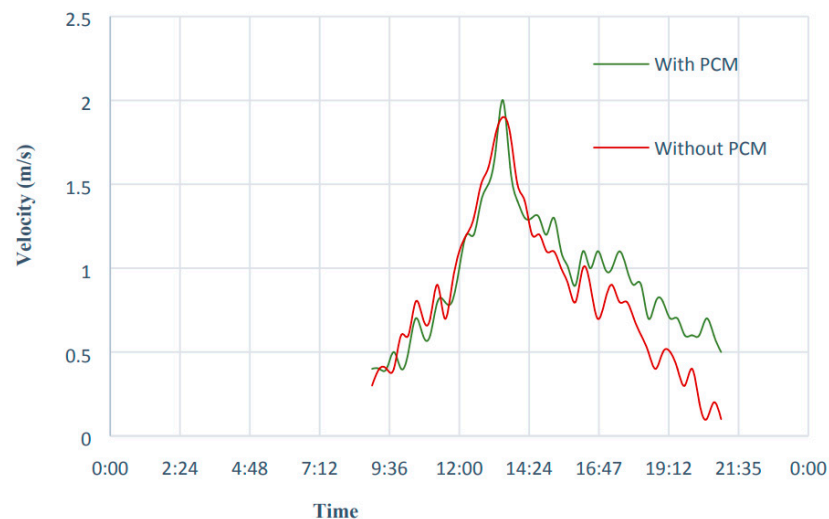


Figure 20. The velocity of the fluid, with and without PCM on August 22nd [100].

Dordelly et al. (2019) [101] explored the effect of adding a PCM (Rubitherm RT44) on the efficiency of two solar chimney prototypes in a laboratory setting, in order to make it a practical option for year-round use. Solar chimneys are known to provide continuous ventilation and improve indoor air quality. The prototype used in this study was made of 2 cm plywood plates with a thermal conductivity of 0.15 W/m K and a size of 3.50 × 1.00 × 0.30 m. After a 6 h charging period, the solar chimney achieved a mean ventilation rate of over 70 m³/h, with a relatively low gain of 550 W/m² from 7 halogen lamps directed towards an effective collector area of 3.00 m². The findings showed that

integrating PCM improved the ventilation rate and slowed the rate of decrease during the discharge phase (6 h) when the halogen lamps did not deliver any energy to the solar chimney, as demonstrated in Figure 21.

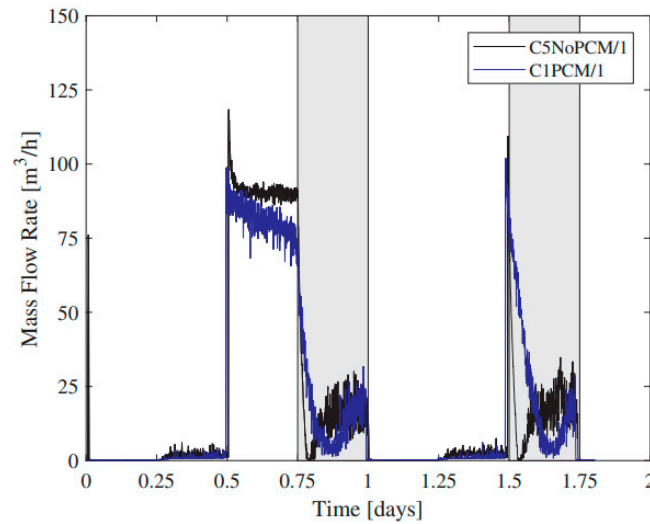


Figure 21. Mass flow rate results under similar operating conditions for C5NoPCM-1 and C1PCM-1 [101].

Tiji et al. (2020) [102] explored the efficiency of a solar chimney with PCM storage (Sodium sulphate decahydrate ($\text{Na}_2\text{SO}_4 \cdot 10\text{H}_2\text{O}$)) with and without fins linked to the absorber plate. The aim was to investigate the velocity and temperature distributions, in addition to the airflow rate inside a room, with and without the PCM and fins, and then compare the results to a non-PCM chimney. The researchers simulated the system using CFD simulation for an entire winter day. The findings indicated that the utilization of PCM has improved the temperature uniformity inside the room but did not reach thermal comfort conditions, with a mean temperature of 14.68°C . To address this, fins were added to the absorber plate, resulting in a 20% improvement in the mean room temperature in comparison to the non-finned case. The results are illustrated in Figure 22.

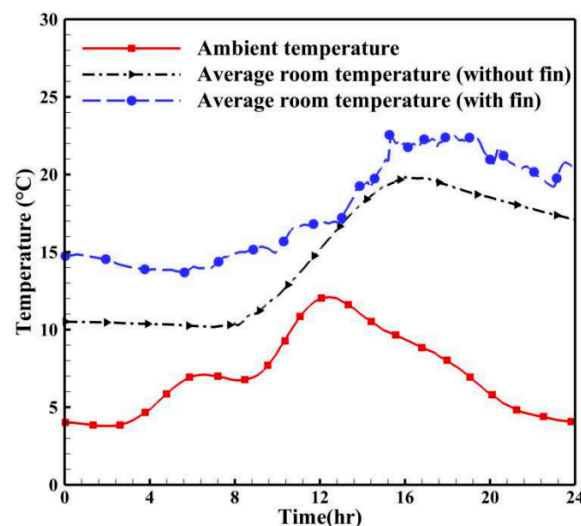


Figure 22. The room’s mean temperature variation for a whole day with PCM in two cases, with and without fin [102].

Phase change capsules (PCC) of paraffin wax are stacked over various sieve beds to create porous layers of heat storage in a new method of phase change heat storage for solar heating reported by Chen and Chen (2020) [103]. The flow of heated air in the

system is propelled by the buoyancy force produced by the solar chimney. The Brinkman–Forchheimer extended Darcy model and double energy equations are used to investigate heat transport and flow in the porous thermal storage layer. The model takes local thermal non-equilibrium (LTNE) in the porous beds into account. Additionally, the impacts of the materials, porosity, and particle size of PCC in the porous thermal storage as well as the features of the flow channel on the thermal storage efficiency are investigated using the k- turbulence model in conjunction with the aforementioned equations. According to the findings, the thermal storage duration of the PCC layer is 7% to 25% longer than that of the Tuff and Basalt layers, as illustrated in Figure 23.

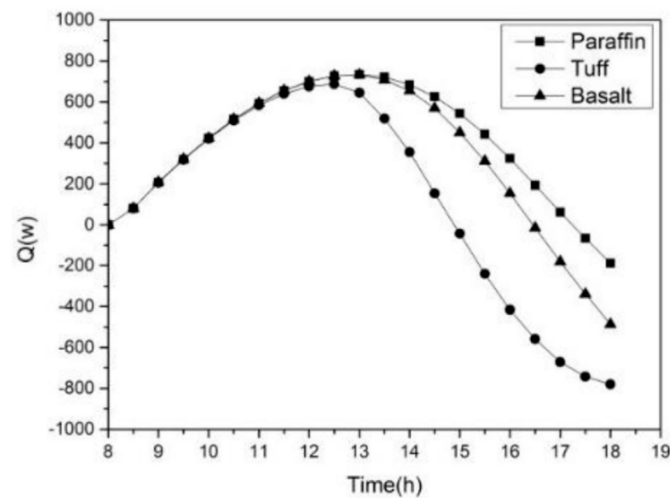


Figure 23. Variation of heat storage capacity with time in the system with different particle materials [103].

Ashouri and Hakkaki-Fard (2021) [104] aimed to improve the performance of an inclined rooftop solar chimney (SC) that integrates PCM and a photovoltaic module (SC-PCM-PV) system. The study examined the efficiency of the system by employing finned absorbers and composite PCMs, and created a 3D-CFD model using the finite volume method. Various design parameters, such as the number and thickness of fins, PCM type (paraffin RT-50, SAT/CF, Pa/CF), and PCM mass were investigated to assess their impact on the length of natural ventilation, ventilation capacity, and power output. This research marks the first time such an investigation has been conducted. The findings demonstrated that raising PCM mass does not considerably lengthen breathing duration but did decrease the ventilation capacity for finless instances. On the contrary, hand, using a finned absorber increases ventilation capacity and duration by 7.7% and 17.6%, respectively. Furthermore, copper-foam-based composite PCMs lengthen the time that the SC-PCM-PV system is ventilated.

Nateghi and Jahangir (2022) [105] conducted a study using Energy Plus to simulate the thermal performance of a house under three different climates. The study included three modes of operation: without solar chimney (SC), with SC, and with SC combined with a layer of PCM. In this regard, the authors used three types of PCMs including the paraffin RT42, RT35, and 25 RT. The study found that incorporating PCM in solar chimneys resulted in lower thermal comfort in hot-arid climates for both heating and ventilation modes. However, in hot-humid and cold semi-arid climates, PCM improved the performance of the SC in providing indoor thermal comfort. The study revealed that the average thermal comfort indices (PMV) improved in hot-humid and cold semi-arid cities by using PCM. The cooling mode of the cold semi-arid climate (Tehran) benefited the most from using PCM.

Li et al. (2022) [106] examined how the inclination angle and heat flux impact the thermal efficiency of a solar chimney with PCM. They varied the heat fluxes (400, 500, and 600 W/m²) and inclination angles (30°, 45°, and 60°), and found that the melting times of the PCM were longer at lower inclination angles and heat fluxes. The inclination angle

had a greater effect on the heat transfer than the heat flux. The solar chimney inclined at 45° had the highest air flow rate, and peak air velocities were 0.27–0.37 m/s during the charging process, and 0.06–0.1 m/s during discharge.

Long et al. (2022) [107] explored a solar chimney-enhanced active hybrid evaporative cooling (SCEAHE) system that incorporated phase change material (PCM) using a verified numerical model. The integration of PCM in the SCEAHE system improved its thermal inertia. According to the modeling results, the absorber surface’s maximum temperature with PCM was 78.8 °C, which was 16.2% lower than its maximum temperature without PCM. The PCM was charged and discharged for roughly 9.5 h (05:30–15:00) and 14.5 h, respectively. Approximately 5 h (15:30–20:30) were spent with the PCM entirely melted, and the solidification of the PCM occurred from 02:00 to 7:15, reaching a maximum of 24% at 05:30. While the highest air flow rate reduced by 17.8% to 209.5 m³/h during the day, the integration of PCM raised the SCEAHE air flow rate by 50% at night. For the SCEAHE with and without PCM, the output air temperatures were from 24.8 to 26.5 °C and from 24.4 to 27.2 °C, respectively.

Overall, it was earlier suggested that the significant variables governing the flow in a solar chimney were $\rho; A; V; q''; c_p; \beta; h_c; g$. In a subsequent work of [108], certain primitive variables were grouped together and presented in Equation (2):

$$\rho AV \frac{V^2}{2} = f^n \left(\rho, g, \frac{q'' A_r}{C_p}, \beta, h_c \right) \tag{2}$$

Additionally, the dimensionless relationship was found to be [109]:

$$\Pi 1 = f^n (\Pi 2) \text{ or } \frac{\frac{1}{2} m \cdot V^2}{\rho h_c^2 g^{\frac{3}{2}}} = f^n \left(\frac{q'' A_r \beta}{\rho C_p h_c^{\frac{5}{2}} g^{\frac{1}{2}}} \right) \tag{3}$$

According to the Buckingham Pi theorem,

$$s = n - b \tag{4}$$

In this case, one dimensionless variable is desired with four basic dimensions [mass (M), length (L), time (t), and temperature (θ)] involved, or $s = 1$ and $b = 4$. Hence, only five quantities are essential.

Equation (1) involves six quantities: $\rho A \frac{V^3}{2}; \rho, g, \frac{q'' A_r}{C_p}, \beta$ and h_c .

Thus, two quantities are selected from among the six to merge into one new term.

The chimney effect, dependent on g and h_c , is among the driving mechanisms in the solar chimney system. Therefore, $g \cdot h_c$ is chosen to be a new variable. Therefore, the pertinent variables are reduced to be [110]:

$$\rho AV \frac{V^2}{2} = f^n \left(\rho, \frac{q'' A_r}{C_p}, \beta, g \cdot h_c \right) \tag{5}$$

A is flow area, ρ is density, V is flow velocity, g is gravitational acceleration, q'' is isolation, A_r is roof area, C_p is specific heat, β is coefficient of volumetric thermal expansion, h_c is chimney height, m is mass flow rate.

The studies related to the usage of phase change material in solar chimneys are displayed in Table 5. The evaluation of the studies in Table 4 shows that the SCEAHE system’s maximum absorber surface temperature with PCM was 78.8 °C, which was 16.2% lower than it was without PCM. For the studied circumstances, the solar chimney with a 45° inclination also had the highest air flow rate. Moreover, using PCM in solar chimneys in both SC functioning modes results in unhappiness in hot arid climates (ventilation and heating).

Table 5. Outline of studies on phase change material for solar chimney.

Authors (Year) [Reference]	Configuration	Type of Study	Studied Parameters	Highlighted Results
Li et al. (2017) [97]	Solar chimney integrated with PCM.	Numerical	Phase change temperature.	The air temperature differential increased from 1.5 to 2 °C and the average mass flow rate increased from 0.033 to 0.038 kg/s as the thermal conductivity of the PCM increased from 0.2 to 0.6 W/m °C, respectively.
Bin et al. (2017) [98]	PCM in the hybrid wall of the solar chimney.	Experimental	The effect of the position of PCM in the hybrid wall.	Without a period of steady temperature, the heat surface temperature of the PCM will rapidly decline during the discharging time (solidification temperature).
Thantong et al. (2018) [99]	A new arrangement of solar chimneys integrating a PCM.	Experimental	Impact of integrating solar chimney with PCM.	Integrating a solar chimney with a PCM is highly effective since it can increase airflow and significantly lower heat gain through the south wall.
Fadaei et al. (2018) [100]	Latent heat storage in a solar chimney pilot.	Experimental	Latent heat storage.	With the SC with PCM and the traditional solar chimney (CSC), the highest absorber surface temperatures are 72 °C and 69 °C, respectively.
Dordelley et al. (2019) [101]	Integrating a Phase Change Material (PCM) in two different laboratory solar chimney prototypes.	Experimental	PCM.	When there is no energy coming from the halogen lamps to the solar chimney (6 h discharge), PCM integration offers a faster ventilation rate and a slower drop.
Tiji et al. (2020) [102]	PCM-enhanced solar chimney with and without considering fins connected to the absorber plate.	Numerical	Impact of using PCM and fins.	Utilizing fins leads to a 20% increase in the room’s mean temperature for the PCM-based solar chimney system in comparison to the non-finned instance.
Chen and Chen (2020) [103]	Novel phase change heat storage for solar heating.	Numerical	Effect of the porosity and particle size in the porous layer.	Enhanced thermal storage efficiency is possible at the system’s ideal ratio of flow channel width to bed thickness, which depends on the porosity and particle size in the porous layer.
Ashouri and Hakkaki-Fard (2021) [104]	A solar chimney system integrated with a PCM and photovoltaic module, installed on an inclined rooftop.	Experimental	Impact of using paraffin/copper foam (Pa/CF) as the PCM.	The utilization of paraffin/copper foam (Pa/CF) as the PCM leads to a power output of 5.54 kWh and ventilation duration of 22 h and 30 min. These values are approximately 16% and 101% higher, respectively, than those obtained with the SC-PV system.

Table 5. Cont.

Authors (Year) [Reference]	Configuration	Type of Study	Studied Parameters	Highlighted Results
Nateghi and Jahangir (2022) [105]	There are three distinct Energy Plus modes: without SC, with SC, and with SC plus a layer of PCM.	Experimental	Effect of combining PCM in solar chimneys.	In hot-arid climates, combining PCM in solar chimneys leads to dissatisfaction in both SC operation modes (ventilation and heating).
Li et al. (2022) [106]	Inclination angle and heat flow on the integrated PCM-based thermal performance of a solar chimney.	Experimental	The inclination angle of SC integrated with PCM.	The solar chimney with a 45° generated the greatest air flow rate.
Long et al. (2022) [107]	PCM-based SCEAHE system.	Experimental	Effect of using PCM.	The SCEAHE system's maximum absorber surface temperature with PCM was 78.8 °C, which is 16.2% lower than without PCM.

3. Critical Evaluation of Utilized PCMs in the Covered Solar Energy Systems

This study discussed the implications of PCMs in different types of solar energy systems including the solar still, solar ponds, solar air heaters, and solar chimneys. The types and thermos-physical characteristics of the PCMs used in solar energy systems are shown in Table 6. Table 6 depicts the melting temperature, latent heat, and thermal conductivity as they play important roles in the utilization of PCMs. As a critical evaluation of the covered studies, it can be stated that the PCMs enable to absorption and store of heat, which efficiently contributes to a reduction in heat loss and an increase in the solar collector system's energy efficiency. Compared to conventional materials, PCMs are able to store more heat which results in more stable energy output. Furthermore, the utilization of PCMs in solar energy systems has resulted in a smaller overall system due to less storage space being needed. System longevity can also be increased the ability of PCMs to lessen thermal stress on the solar collector system. More importantly, the PCMs can lessen energy expenses by minimizing the need for backup energy sources at times of poor solar energy availability. However, the addition of PCMs to the solar collector system may result in an increase in the system's initial cost, which could make it less affordable for some consumers. Additionally, PCMs can only store thermal energy within a certain temperature range, they are less effective at extremely hot or cold temperatures. The longevity of the system is quite related to the number of heat cycles that PCMs can withstand before degrading. Notably, the routine maintenance for the solar collector system is vital to guarantee optimal performance, which in turn would increase the operational cost. There is also a necessity for additional space for energy storage, and therefore the overall system design may be affected. Beyond the above demerits, the PCMs have low thermal conductivity coefficients, which reduce the heat storage and release during melting and crystallization operations and thus exhibit relatively large volume changes during phase transitions.

Table 6 shows the existence of several other effective PCMs with competent thermal conductivity larger than 1 W/m K and substantial latent heat, in contrast to a significant number of PCMs with poor thermal conductivity. In order to protect the PCM from moisture and other environmental variables, it is crucial to use these materials for future research and optimization. By using particular methods such as fins and heat exchangers, the heat exchange between the PCM and the environment should also be increased. The addition of thermally conductive fillers, such as carbon nanotubes, graphene, or metal particles, can also boost the thermal conductivity and latent heat of PCMs. Another crucial issue that needs to be taken into account is the PCMs' melting temperature. In general, PCMs with higher melting temperatures have more energy to store. This implies that they have greater energy storage capacity per unit of mass or volume, which may be helpful in particular applications. Additionally, PCMs with higher melting points typically have better thermal stability, which means they can hold onto their properties for a longer time. In fact, a PCM's latent heat directly correlates to how much energy it can store or release during a phase shift. In comparison to PCMs with lower latent heats, those with higher latent heats can store or release more energy per unit of mass or volume. A balance between the desired thermal properties and other factors, most importantly the energy storage capacity, must be found. Beyond this, it should be acknowledged that the higher thermal conductivity values may come with tradeoffs, such as reduced energy storage capacity or increased costs. In this regard, the choice of whether to raise or lower a PCM's melting temperature should be made based on the application's needs. This is because PCMs with high melting temperatures are likely to have low thermal conductivity. Finally, since PCMs' molecular structure directly affects their thermal conductivity, future research should focus on determining what that structure should be. For instance, altering the PCM chains' length and branching might enhance the passage of heat between molecules.

Table 6. Overview of types and thermos-physical characteristics of PCMs used in solar applications.

Type of PCM	Range of Melting Temperature (°C)	Range of Latent Heat Capacity (J/g)	Thermal Conductivity (W/m K)	Authors (Year) [Reference]
Commercial-grade paraffin wax	47–68	160–220	≤0.2 *	Feliński and Sekret (2016) [25]
n-eicosane micro-encapsulated PCM) suspended in water or a mixture of water and glycol	36–38	195	0.23	Serale et al. (2016) [26]
Erythritol and expanding graphite (0–4 wt.%)	130.45–129.56	320.7–308.8	0.703–2.674	Li and Zhai (2017) [27]
Microencapsulated phase change material of paraffin@melamine resin mixed in an ethanol/water mixture	42.5–49.8	166	-	Wang et al. (2019) [28]
PCM was encapsulated in spherical particles and made of 20% high-purity graphite and 80% natural grease	15–70	190–210	3–5	Wang et al. (2019) [29]
A microcapsule of an octadecane core and a melamine-formaldehyde resin shell with graphene oxide and oleic acid-coated Fe ₃ O ₄ magnetic nanoparticles in the shell (rGO-MPCMs)	25.82–28.34	73.05	0.4076	Gao et al. (2020) [30]
PCM1: Ecopetrol Semirefinada PCM, and PCM2: Rubitherm RT-47 PCM	60, 41–46	210, 160	0.9, 0.2	Palacio et al. (2020) [31]
PCM1: Paraffin wax + 1% nano-Cu, and PCM2: paraffin wax + 2% nano-Cu	59.57, 59.14	160.3, 172.2	0.196, 0.226	Elarem et al. (2021) [32]
PCM1: Medical paraffin and PCM2: grade A paraffin waxes with ZnO micro-particles or 5 wt% CuO nanoparticles	45, 64	190, 268	0.21, 0.211	Alshukri et al. (2021) [33]
Shape-stabilized PCM of sodium phosphate monohydrate, sodium acetate trihydrate, expandable graphite and carboxymethylcellulose	55–57	193.62	-	Sadeghi et al. (2022) [34]
Shape-stabilized PCM of sodium acetate trihydrate and salt hydrate	57	218.5	1.5	Yeh et al. (2022) [35]
Encapsulated spherical capsules and a synthetic oil	280–380	75–266	0.5–0.92	Nekoonam and Ghasempour (2022) [36]
Decane PCM and glass (amorphous silica)	-	-	0.74	Hatamleh et al. (2022) [38]
Composite of paraffin wax with 0.33 wt% nano-copper	51.2	227	0.31	Algarni et al. (2020) [39]
CuO/water nanofluid, CuO/ethylene glycol nanofluid, binary (CuO + Al ₂ O ₃)/water nanofluid, binary (CuO + Al ₂ O ₃)/EG nanofluid in two different volume fractions, and CuO/water nanofluid	36.85	192.66	0.749	Karami et al. (2023) [40]

Table 6. Cont.

Type of PCM	Range of Melting Temperature (°C)	Range of Latent Heat Capacity (J/g)	Thermal Conductivity (W/m K)	Authors (Year) [Reference]
Tritriacontane paraffin PCM and copper metal foam	72	256	0.21	Pawar and Sobhansarbandi (2023) [41]
Shape-stabilised PCM of 5 wt% expanded graphite	46	195	1.5	Cheng et al. (2019) [44]
PCM1: paraffin wax and PCM2: two PCMs of different phase change temperature ranges	58.03–64.5, 53.05–62	-	-	Vigneswaran et al. (2019) [45]
Three PCMs: Sodium thiosulfate pentahydrate, sodium acetate trihydrate, and paraffin wax	48.5, 58, 56–58	208.8, 265, 226	0.16–0.37, 1.44, 0.2–0.3	Abu-Arabi et al. (2020) [46]
PCM1: and PCM2: hollow cylindrical pin fins embedded in the PCM	56–58, 60.85	-	-	Yousef et al. (2019) [47]
12 aluminum tubes with paraffin wax with copper rods	-	226	-	Elashmawy et al. (2020) [48]
Copper tubes filled with paraffin were as PCM	56	-	0.24	Kabeel et al. (2020) [49]
TH-ME 58 (SiO ₂ -paraffin))	46.06–62.49	153.76	0.287	Chen et al. (2021) [50]
A commercialized inorganic salt hydrate + water + Additive PCM (Product number: PGSCR Co. PCM28/315)	28	225	0.6 ± 15%	Jahanpanah et al. (2021) [51]
Paraffin wax combined with copper oxide nanoparticles (975 g PCM + 25 g CuO)	53	187	0.28	Abdullah et al. (2022) [55]
Paraffin wax and 3 wt% Al ₂ O ₃	56–58	226	0.24	Tuly et al. (2022) [56]
0.5–2.5 wt% of 40 nm sized Zn-nanoparticle and 5 kg paraffin PCM	36–42	-	0.3398–0.4001	Afolabi et al. (2023) [57]
Paraffin wax	54.5	190	0.24	Bacha et al. (2023) [58]
4 PCMs including the n-pentacosane, n-hexacosane, n-docosane and n-tetracosane.	54, 56, 44, 51	238, 257, 249, 255	0.21, 0.21, 0.21, 0.21	Amirifard et al. (2018) [62]
Paraffin wax	46	210	-	Beik et al. (2019) [64]
Paraffin wax 50 and paraffin wax 60	48–50, 58–60	171.1, 213.8	0.2, 0.2	Wang et al. (2020) [65]
Paraffin wax	41–44	255	0.2	Rghif et al. (2021) [66]

Table 6. Cont.

Type of PCM	Range of Melting Temperature (°C)	Range of Latent Heat Capacity (J/g)	Thermal Conductivity (W/m K)	Authors (Year) [Reference]
Paraffin waxes of RT35 HC and RT44 HC	34–36, 41–44	240, 250	0.2, 0.2	Colarossi et al. (2022) [67]
RT 50 and RT 60 paraffin waxes	less than 55	171.1, 213.8	0.215, 0.212	Wang et al. (2022) [69]
Paraffin wax	46	210	-	Reza et al. (2022) [70]
Paraffin wax	54	190	0.21	Kabeel et al. (2016) [73]
Paraffin wax	56–60	214.4	0.21	El Khadraoui et al. (2017) [74]
Paraffin wax	38–43	174	0.2	Salih et al. (2019) [75]
Paraffin wax	58–60	180.8	0.241	Raj et al. (2019) [77]
Paraffin wax type RT70HC (RUBITHERM)	69	260	0.2	Mahdi et al. (2021) [80]
Three PCMs of paraffin wax, n-octadecane, and calcium chloride hexahydrate	64, 30, 30	268.336, 245, 170	0.21, 0.358, 1.09	Madhulatha et al. (2021) [81]
HS29 PCM	26–29	190	1.05	Abu-Hamdeh et al. (2022) [83]
Rubitherm RT 45	41–46	160	0.2	Palacio et al. (2022) [84]
Paraffin RT58	58	180	0.2	Chaatouf et al. (2022) [85]
Paraffin wax RT42	38–43	-	0.2	Verma et al. (2022) [86]
Paraffin wax	58–60	214.4	0.2	Sharol et al. (2022) [87]
PCM-rod (ZN-110H)	54.4	147.7	0.9	Luo et al. (2002) [88]
Interlayer ventilated phase change material of PCM24 and EGPCM	29.81, 26.32	216.05–214.23, 172.36–164.89	0.22, 0.81	He et al. (2022) [91]
Acetamide, stearic acid, and paraffin wax	112.8, 63.4, 65.8	210.21, 200.7, 198.7	0.592, 0.18, 0.24	Brahma et al. (2023) [92]

Table 6. Cont.

Type of PCM	Range of Melting Temperature (°C)	Range of Latent Heat Capacity (J/g)	Thermal Conductivity (W/m K)	Authors (Year) [Reference]
Paraffin RT 42	38–43	174	0.2	Li et al. (2017) [97]; Thantong et al. (2018) [99]
paraffin wax (C ₂₀)	44–46	189	0.21	Fadaei et al. (2018) [100]
Rubitherm RT44	41–44	250	0.15	Dordelly et al. (2019) [101]
Sodium sulphate decahydrate (Na ₂ SO ₄ ·10H ₂ O)	33.85	126	-	Tiji et al. (2020) [102]
Paraffin wax	28.85–30.85	-	0.36	Chen and Chen (2020) [103]
Paraffin RT-50, SAT/CF, Pa/CF	50, 56.75, 42.67	160, 271, 270.7	0.2, 3.4, 6.2	Ashouri and Hakkaki-Fard (2021) [104]
Three PCMs of paraffin RT42, RT35, and 25 RT	38–43, 34–36, 22–26	174, 157, 148	0.2, 0.2, 0.19	Nateghi and Jahangir (2022) [105]; Li et al. (2022) [106]; Long et al. (2022) [107]

*: Ukrainczyk et al. 2010 [111].

4. Conclusions

Solar energy is an attractive alternative that helps to reduce reliance on non-renewable energy sources. Among renewable solar energy applications, domestic solar water heating systems (DSWHS) are widely used. However, these systems face challenges, the primary one being the inability to provide sufficient hot water on demand due to reduced solar radiation during nighttime or cloudy days. This review study focused on the current implications of PCMs in different solar thermal energy systems. The following conclusions are made after reviewing more than 90 relevant studies and analyzing their results:

1. Solar collector: Adding fins significantly affects the ETSC's ability to transfer heat from the paraffin during its phase transition. It was discovered that as the fins' thickness decreases, the PCM melts more quickly. Additionally, it was found that adding 1% Cu to the PCM was the ideal mass concentration for raising the HTF output temperature by 2 K.
2. Solar collector: The storage efficiency for mid-temperature use was increased by more than 40% as a result of using PCM.
3. Solar still: Due to their larger effective heat capacities, droplets with MPCM may experience a slower temperature drop during the flash evaporation process.
4. Solar still: The SSPCM-equipped solar still entails an increase in productivity of less than 44% beyond the productivity of the standard solar still.
5. Solar bond: A solar pond containing Al_2O_3 nanoparticles was capable of providing hot water till 7:30 p.m. in the evening.
6. Solar bond: The temperature difference decreased as a result of the PCM-induced fall in the pond's maximum temperature, even though both ponds' minimum temperatures were roughly similar.
7. Solar air heater: Using PCM in the solar air heater eventually reduced annual energy consumption.
8. Solar air heater: Employing PCMs with greater melting point temperatures causes SAH outlet temperatures to rise by nearly 5 °C and their daily performance to drop insignificantly (by approximately 3%).
9. Solar air heater: The increased airflow velocity causes the melting time to take longer to complete and lowers the paraffin's melting temperature.
10. Chimney: When fins are used in the PCM-based solar chimney system, the mean temperature of the room is 20% higher than in the non-finned scenario.
11. Chimney: Without a period of steady temperature, the heat surface temperature of the PCM will rapidly decline throughout the discharging time (solidification temperature).
12. Chimney: When paraffin/copper foam (Pa/CF) is used as the PCM instead of the SC-PV system, the power output (5.54 kWh) and ventilation time (22 h and 30 min), respectively, are the highest.

5. Recommendation for Future Work

Despite the many benefits of solar energy, it is mainly characterized by its features of discontinuities and instability. To address these shortcomings, numerous researchers have combined solar energy applications with thermal energy storage technology. In recent years, latent heat storage has drawn a lot of interest. Some advantages of the material include a high energy density and nearly isothermal operation during both melting and solidification. For many years, PCM preparation and heat exchanger design were the principal topics of latent heat storage research [112]. Certain elements with high thermal conductivity are mixed into PCMs to create a new composite material because many PCMs have low thermal conductivity, which negatively impacts heat charge and discharge. The following recommendations are given for additional research:

1. In the future, the solar pond could additionally utilize other organic PCMs for capsule manufacturing, such as fatty acids, polyglycerol, and capric acids.

2. To assure large and beneficial social consequences, more research is required on the development of efficient and affordable PCMs with reduced ageing effects for solar thermal energy storage applications.
3. It is required to enhance the properties of PCM such as the conductivity parameter for better results.
4. Advanced research in the materials science of PCMs can enable innovative engineering solutions to integrate PCMs into solar thermal systems, aligning with the clean energy roadmap.
5. PCMs can have better thermal stability, less leakage, and longer durability if they are perfectly encapsulated.
6. The total effectiveness and stability of the solar energy system can be increased by combining PCM technology with other energy storage technologies, such as batteries or super-capacitors.

Author Contributions: Conceptualization, F.L.R. and M.A.A.-O.; methodology, F.L.R. and A.H.; software, H.Y.B.; validation, F.L.R., H.Y.B. and A.H.; formal analysis, M.A.A.-O. and H.Y.B.; investigation, F.L.R.; resources, A.D. and A.H.; data curation, F.L.R., A.D. and M.A.A.-O.; writing—original draft preparation, F.L.R., M.A.A.-O., A.D., H.Y.B. and A.H.; writing—review and editing, F.L.R., M.A.A.-O., A.D., H.Y.B. and A.H.; visualization, F.L.R.; supervision, F.L.R. and A.H.; project administration, F.L.R. and A.D.; funding acquisition, A.H. and A.D. All authors have read and agreed to the published version of the manuscript.

Funding: This research received no external funding.

Data Availability Statement: Not applicable.

Acknowledgments: The financial support of Kerbala University and University of Warith Al-Anbiyaa Universities in Iraq is gratefully acknowledged.

Conflicts of Interest: The authors declare no conflict of interest.

Abbreviations

Symbol	Definition
CSS	Conventional solar still
DSSS	Double-slope solar still
ETSC	Evacuated tube solar collector
ETC/S	Evacuated tube collector/storage
FPSC	Flat plate solar collector
HPETC	Heat pipe evacuated tube collector
HTF	Heat transfer fluid
LHTES	Latent heat thermal energy storage
MCVTSD	Modified convex tubular solar distiller
MWCNT	Multi-walled carbon nanotube
PCMs	Phase change materials
PCS	Slurry phase change materials
SPTR	Solar parabolic trough reflector
SSPCM	Shape-stabilized phase change material
TESS	Thermal energy storage system

References

1. Perlin, J. *Let It Shine: The 6000-Year Story of Solar Energy*; New World Library: Novato, CA, USA, 2013.
2. Daniels, F.; Duffie, J. *Solar Energy Research*; University of Wisconsin Press: Madison, WI, USA, 1955.
3. Bhushan, B.; Singh, R. A review on methodology of artificial roughness used in duct of solar air heaters. *Energy* **2010**, *35*, 202–212. [[CrossRef](#)]
4. Zhao, D.L.; Li, Y.; Dai, Y.J.; Wang, R.Z. Optimal study of a solar air heating system with pebble bed energy storage. *Energy Convers. Manag.* **2011**, *52*, 2392–2400. [[CrossRef](#)]
5. Ghoneim, A.; Klein, S.; Duffie, J. Analysis of collector storage building walls using phase change materials. *Sol. Energy* **1991**, *47*, 237–242. [[CrossRef](#)]

6. Pasupathy, A.; Athanasius, L.; Velraj, R.; Seeniraj, R. Experimental investigation and numerical simulation analysis on the thermal performance of a building roof incorporating phase change material (PCM) for thermal management. *Appl. Thermal Eng.* **2008**, *28*, 556–565. [\[CrossRef\]](#)
7. Bland, A.; Khzouz, M.; Statheros, T.; Gkanas, E. PCMs for residential building applications: A short review focused on disadvantages and proposals for future development. *Buildings* **2017**, *7*, 78. [\[CrossRef\]](#)
8. Al-Yasiri, Q.; Szabó, M. Paraffin as a phase change material to improve building performance: An overview of applications and thermal conductivity enhancement techniques. *Renew. Energy Environ. Sustain.* **2021**, *6*, 38. [\[CrossRef\]](#)
9. Khedher, N.B.; Bantan, R.A.; Kolsi, L.; Omri, M. Performance investigation of a vertically configured LHTEs via the combination of nano-enhanced PCM and fins: Experimental and numerical approaches. *Int. Commun. Heat Mass Transf.* **2022**, *137*, 106246. [\[CrossRef\]](#)
10. Fan, Y.; Zhang, X.; Wang, X.; Li, J.; Zhu, Q. Super-cooling prevention of microencapsulated phase change material. *Thermochim. Acta* **2004**, *413*, 1–6. [\[CrossRef\]](#)
11. Yamagishi, Y.; Sugeno, T.; Ishige, T.; Takeuchi, H.; Pyatenko, A.T. An evaluation of microencapsulated PCM for use in cold energy transportation medium. In Proceedings of the 31st Intersociety Energy Conversion Engineering Conference, Washington, DC, USA, 11–16 August 1996; pp. 2077–2083.
12. Jin, Y.; Wan, Q.; Ding, Y. PCMs heat transfer performance enhancement with expanded graphite and its thermal stability. *Proc. Eng.* **2015**, *102*, 1877–1884. [\[CrossRef\]](#)
13. Letcher, T.M.; Law, R.; Reay, D. *Storing Energy: With Special Reference to Renewable Energy Sources*; Elsevier: Oxford, UK, 2016.
14. Sittisart, P.; Farid, M.M. Fire retardants for phase change materials. *Appl. Energy* **2011**, *88*, 3140–3145. [\[CrossRef\]](#)
15. Song, G.; Ma, S.; Tang, G.; Yin, Z.; Wang, X. Preparation and characterization of flame retardant form-stable phase change materials composed by EPDM, paraffin and nano magnesium hydroxide. *Energy* **2010**, *35*, 2179–2183. [\[CrossRef\]](#)
16. Nazir, H.; Batool, M.; Osorio, F.J.B.; Isaza-Ruiz, M.; Xu, X.; Vignarooban, K.; Phelan, P.; Kannan, A.M. Recent developments in phase change materials for energy storage applications: A review. *Int. J. Heat Mass Transf.* **2019**, *129*, 491–523. [\[CrossRef\]](#)
17. Sikiru, S.; Oladosu, T.L.; Aмоса, T.I.; Kolawole, S.Y.; Soleimani, H. Recent advances and impact of phase change materials on solar energy: A comprehensive review. *J. Energy Storage* **2022**, *53*, 105200. [\[CrossRef\]](#)
18. Cabeza, L.F.; Ibanez, M.; Sole, C.; Roca, J.; Nogues, M. Experimentation with a water tank including a PCM module. *Sol. Energy Mater. Sol. Cells* **2006**, *90*, 1273–1282. [\[CrossRef\]](#)
19. Chaurasia, P.B.L. Phase change material in solar water heater storage system. In Proceedings of the 8th International Conference on Thermal Energy Storage, Stuttgart, Germany, 28 August–1 September 2000.
20. Canbazoglu, S.; Sahinbaslan, A.; Ekmekyapar, A.; Aksoy, Y.G.; Akarsu, F. Enhancement of solar thermal energy storage performance using sodium thiosulfate pentahydrate of a conventional solar water-heating system. *Energy Build.* **2005**, *37*, 235–242. [\[CrossRef\]](#)
21. Hailiot, D.; Franquet, E.; Gibout, S.; Bedecarrats, J.P. Optimization of solar DHW system including PCM media. *Appl. Energy* **2013**, *109*, 470e5. [\[CrossRef\]](#)
22. Hussain, F.; Othman, M.Y.H.; Sopian, K.; Yatim, B.; Ruslan, H.; Othman, H. Design development and performance evaluation of photovoltaic/thermal (PV/T) air base solar collector. *Renew. Sustain. Energy Rev.* **2013**, *25*, 431–441. [\[CrossRef\]](#)
23. Rashidov, Y.K.; Ramankulov, S.A. Improving the Efficiency of Flat Solar Collectors in Heat Supply Systems. *Cent. Asian J. Theor. Appl. Sci.* **2021**, *2*, 152–159.
24. Alshukri, M.J.; Hussein, A.K.; Eidan, A.A.; Alsabery, A.I. A review on applications and techniques of improving the performance of heat pipe-solar collector systems. *Solar Energy* **2022**, *236*, 417–433. [\[CrossRef\]](#)
25. Feliński, P.; Sekret, R. Experimental study of evacuated tube collector/storage system containing paraffin as a PCM. *Energy* **2016**, *114*, 1063–1072. [\[CrossRef\]](#)
26. Serale, G.; Goia, F.; Perino, M. Numerical model and simulation of a solar thermal collector with slurry Phase Change Material (PCM) as the heat transfer fluid. *Solar Energy* **2016**, *134*, 429–444. [\[CrossRef\]](#)
27. Li, B.; Zhai, X. Experimental investigation and theoretical analysis on a mid-temperature solar collector/storage system with composite PCM. *Appl. Therm. Eng.* **2017**, *124*, 34–43. [\[CrossRef\]](#)
28. Wang, Z.; Qu, J.; Zhang, R.; Han, X.; Wu, J. Photo-thermal performance evaluation on MWCNTs-dispersed microencapsulated PCM slurries for direct absorption solar collectors. *J. Energy Storage* **2019**, *26*, 100793. [\[CrossRef\]](#)
29. Wang, D.; Liu, H.; Liu, Y.; Xu, T.; Wang, Y.; Du, H.; Wang, X.; Liu, J. Frost and High-temperature resistance performance of a novel dual-phase change material flat plate solar collector. *Sol. Energy Mater. Sol. Cells* **2019**, *201*, 110086. [\[CrossRef\]](#)
30. Gao, G.; Zhang, T.; Jiao, S.; Guo, C. Preparation of reduced graphene oxide modified magnetic phase change microcapsules and their application in direct absorption solar collector. *Sol. Energy Mater. Sol. Cells* **2020**, *216*, 110695. [\[CrossRef\]](#)
31. Palacio, M.; Rincón, A.; Carmona, M. Experimental comparative analysis of a flat plate solar collector with and without PCM. *Solar Energy* **2020**, *206*, 708–721. [\[CrossRef\]](#)
32. Elarem, R.; Alqahtani, T.; Mellouli, S.; Aich, W.; Ben Khedher, N.; Kolsi, L.; Jemni, A. Numerical study of an Evacuated Tube Solar Collector incorporating a Nano-PCM as a latent heat storage system. *Case Stud. Therm. Eng.* **2021**, *24*, 100859. [\[CrossRef\]](#)
33. Alshukri, M.J.; Eidan, A.A.; Najim, S.I. The influence of integrated Micro-ZnO and Nano-CuO particles/paraffin wax as a thermal booster on the performance of heat pipe evacuated solar tube collector. *J. Energy Storage* **2021**, *37*, 102506. [\[CrossRef\]](#)
34. Sadeghi, G.; Mehrali, M.; Shahi, M.; Brem, G.; Mahmoudi, A. Experimental analysis of Shape-Stabilized PCM applied to a Direct-Absorption evacuated tube solar collector exploiting sodium acetate trihydrate and graphite. *Energy Convers. Manag.* **2022**, *269*, 116176. [\[CrossRef\]](#)

35. Yeh, C.-Y.; Boonk, K.; Sadeghi, G.; Mehrali, M.; Shahi, M.; Brem, G.; Mahmoudi, A. Experimental and numerical analysis of thermal performance of shape stabilized PCM in a solar thermal collector. *Case Stud. Therm. Eng.* **2022**, *30*, 101706. [[CrossRef](#)]
36. Nekoonam, S.; Ghasempour, R. Modeling and optimization of a thermal energy storage unit with cascaded PCM capsules in connection to a solar collector. *Sustain. Energy Technol. Assess.* **2022**, *52*, 102197. [[CrossRef](#)]
37. Wen, X.; Ji, J.; Li, Z.; Song, Z. Performance analysis of a concentrated system with series photovoltaic/thermal module and solar thermal collector integrated with PCM and TEG. *Energy* **2022**, *249*, 123777. [[CrossRef](#)]
38. Hatamleh, R.I.; Abu-Hamdeh, N.H.; Khoshaim, A.; Alzahrani, M.A. Using phase change material (PCM) to improve the solar energy capacity of glass in solar collectors by enhancing their thermal performance via developed MD approach. *Eng. Anal. Bound. Elem.* **2022**, *143*, 163–169. [[CrossRef](#)]
39. Algarni, S.; Mellouli, S.; Alqahtani, T.; Almutairi, K.; Khan, A.; Anqi, A. Experimental investigation of an evacuated tube solar collector incorporating nano-enhanced PCM as a thermal booster. *Appl. Therm. Eng.* **2020**, *180*, 115831. [[CrossRef](#)]
40. Karami, M.; Shahini, N.; Behabadi, M.A.A. Numerical investigation of double-walled direct absorption evacuated tube solar collector using microencapsulated PCM and nanofluid. *J. Mol. Liq.* **2023**, *377*, 121560. [[CrossRef](#)]
41. Pawar, V.R.; Sobhansarbandi, S. Heat transfer enhancement of a PCM-porous metal based heat pipe evacuated tube solar collector: An experimental study. *Sol. Energy* **2023**, *251*, 106–118. [[CrossRef](#)]
42. Rashid, F.L.; Al-Obaidi, M.A.; Hussein, A.K.; Akkurt, N.; Ali, B.; Younis, O. Floating solar stills and floating solar-driven membranes: Recent advances and overview of designs, performance and modern combinations. *Solar Energy* **2022**, *247*, 355–372. [[CrossRef](#)]
43. Hussein, A.K.; Rashid, F.L.; Abed, A.M.; Al-Khaleel, M.; Togun, H.; Ali, B.; Akkurt, N.; Malekshah, E.H.; Biswal, U.; Al-Obaidi, M.A.; et al. Inverted Solar Stills: A Comprehensive Review of Designs, Mathematical Models, Performance, and Modern Combinations. *Sustainability* **2022**, *14*, 13766. [[CrossRef](#)]
44. Cheng, W.-L.; Huo, Y.-K.; Nian, Y.-L. Performance of solar still using shape-stabilized PCM: Experimental and theoretical investigation. *Desalination* **2019**, *455*, 89–99. [[CrossRef](#)]
45. Vigneswaran, V.; Kumaresan, G.; Dinakar, B.; Kamal, K.K.; Velraj, R. Augmenting the productivity of solar still using multiple PCMs as heat energy storage. *J. Energy Storage* **2019**, *26*, 101019. [[CrossRef](#)]
46. Abu-Arabi, M.; Al-Harashsheh, M.; Ahmad, M.; Mousa, H. Theoretical modeling of a glass-cooled solar still incorporating PCM and coupled to flat plate solar collector. *J. Energy Storage* **2020**, *29*, 101372. [[CrossRef](#)]
47. Yousef, M.S.; Hassan, H.; Kodama, S.; Sekiguchi, H. An experimental study on the performance of single slope solar still integrated with a PCM-based pin-finned heat sink. *Energy Procedia* **2019**, *156*, 100–104. [[CrossRef](#)]
48. Elashmawy, M.; Alhadri, M.; Ahmed, M.M. Enhancing tubular solar still performance using novel PCM-tubes. *Desalination* **2021**, *500*, 114880. [[CrossRef](#)]
49. Kabeel, A.; Abdelgaied, M.; Harby, K.; Eisa, A. Augmentation of diurnal and nocturnal distillate of modified tubular solar still having copper tubes filled with PCM in the basin. *J. Energy Storage* **2020**, *32*, 101992. [[CrossRef](#)]
50. Chen, Q.; Xu, G.; Xia, P. The performance of a solar-driven spray flash evaporation desalination system enhanced by microencapsulated phase change material. *Case Stud. Therm. Eng.* **2021**, *27*, 101267. [[CrossRef](#)]
51. Jahanpanah, M.; Sadatinejad, S.J.; Kasaeian, A.; Jahangir, M.H.; Sarrafha, H. Experimental investigation of the effects of low-temperature phase change material on single-slope solar still. *Desalination* **2021**, *499*, 114799. [[CrossRef](#)]
52. Gnanavel, C.; Saravanan, R.; Chandrasekaran, M. CFD analysis of solar still with PCM. *Mater. Today Proc.* **2021**, *37*, 694–700. [[CrossRef](#)]
53. Hansen, R.S.; Mary, M.B.Q.; Subramanian, S.S.; Raj, J.A.; Gnanaraj, S.J.P.; Appadurai, M. Utilization of PCM in inclined and single basin solar stills to improve the daily productivity. *Mater. Today Proc.* **2022**, *62*, 967–972. [[CrossRef](#)]
54. Ajdari, H.; Ameri, A. Performance assessment of an inclined stepped solar still integrated with PCM and CuO/GO nanocomposite as a nanofluid. *J. Build. Eng.* **2022**, *49*, 104090. [[CrossRef](#)]
55. Abdullah, A.; Omara, Z.; Essa, F.A.; Alqsair, U.F.; Aljagham, M.; Mansir, I.B.; Shanmugan, S.; Alawee, W.H. Enhancing trays solar still performance using wick finned absorber, nano-enhanced PCM. *Alex. Eng. J.* **2022**, *61*, 12417–12430. [[CrossRef](#)]
56. Tuly, S.; Ayon, A.; Hassan, R.; Das, B.K.; Khan, R.; Sarker, M. Performance investigation of active double slope solar stills incorporating internal sidewall reflector, hollow circular fins, and nanoparticle-mixed phase change material. *J. Energy Storage* **2022**, *55*, 105660. [[CrossRef](#)]
57. Afolabi, L.O.; Enweremadu, C.C.; Kareem, M.; Arogundade, A.I.; Irshad, K.; Islam, S.; Oladosu, K.; Elfaghi, A.M.; Didane, D.H. Experimental investigation of double slope solar still integrated with PCM nanoadditives microencapsulated thermal energy storage. *Desalination* **2023**, *553*, 116477. [[CrossRef](#)]
58. Ben Bacha, H.; Abdullah, A.; Kabeel, A.E.; Abdelgaied, M. Design and development of a tubular solar distiller using a convex absorber, wick materials, and PCM reservoir combined with a solar parabolic concentrator. *J. Energy Storage* **2023**, *62*, 106897. [[CrossRef](#)]
59. Shahid, M.I.; Asim, M.; Farhan, M.; Sheikh, M.F.; Ashraf, M.U.; Arshad, H.; Alghamdi, A.; Alshahrani, A.; Bahaddad, A.A.; Almarhabi, K.A. Design and performance analysis of salinity gradient solar pond under different climatic and soil conditions. *PLoS ONE* **2023**, *18*, e0279311. [[CrossRef](#)]
60. Kumar, A.; Singh, K.; Verma, S.; Das, R. Inverse prediction and optimization analysis of a solar pond powering a thermoelectric generator. *Solar Energy* **2018**, *169*, 658–672. [[CrossRef](#)]
61. Sarathkumar, P.; Sivaram, A.; Rajavel, R.; Kumar, R.P.; Krishnakumar, S. Experimental Investigations on The Performance of A Solar Pond by using Encapsulated Pcm with Nanoparticles. *Mater. Today Proc.* **2017**, *4*, 2314–2322. [[CrossRef](#)]

62. Amirifard, M.; Kasaeian, A.; Amidpour, M. Integration of a solar pond with a latent heat storage system. *Renew. Energy* **2018**, *125*, 682–693. [[CrossRef](#)]
63. Ines, M.; Paolo, P.; Roberto, F.; Mohamed, S. Experimental studies on the effect of using phase change material in a salinity-gradient solar pond under a solar simulator. *Solar Energy* **2019**, *186*, 335–346. [[CrossRef](#)]
64. Beik, A.J.G.; Assari, M.R.; Tabrizi, H.B. Transient modeling for the prediction of the temperature distribution with phase change material in a salt-gradient solar pond and comparison with experimental data. *J. Energy Storage* **2019**, *26*, 101011. [[CrossRef](#)]
65. Wang, H.; Xiaomeng, M.; Liugang, Z.; Zhang, X.; Mei, Y.; Zhang, A. Numerical and experimental study of effect of paraffin phase change heat storage capsules on the thermal performance of the solar pond. *Energy Explor. Exploit.* **2020**, *39*, 1010–1023. [[CrossRef](#)]
66. Rghif, Y.; Zeghmami, B.; Bahraoui, F. Modeling the influences of a phase change material and the Dufour effect on thermal performance of a salt gradient solar pond. *Int. J. Therm. Sci.* **2021**, *166*, 106979. [[CrossRef](#)]
67. Colarossi, D.; Pezzuto, M.; Principi, P. Effect of PCM melting temperature on solar ponds performance: Design and experimental investigation. *Solar Energy* **2022**, *242*, 225–233. [[CrossRef](#)]
68. Colarossi, D.; Principi, P. Experimental investigation and optical visualization of a salt gradient solar pond integrated with PCM. *Sol. Energy Mater. Sol. Cells* **2022**, *234*, 111425. [[CrossRef](#)]
69. Wang, H.; Zhang, C.Y.; Zhang, L.G. Effect of steel-wires and paraffin composite phase change materials on the heat exchange and exergetic performance of salt gradient solar pond. *Energy Rep.* **2022**, *8*, 5678–5687. [[CrossRef](#)]
70. Assari, M.R.; Beik, A.J.G.; Eydi, R.; Tabrizi, H.B. Thermal-salinity performance and stability analysis of the pilot salt-gradient solar ponds with phase change material. *Sustain. Energy Technol. Assess.* **2022**, *53*, 102396. [[CrossRef](#)]
71. Tchinda, R. A review of the mathematical models for predicting solar air heaters systems. *Renew. Sustain. Energy Rev.* **2009**, *13*, 1734–1759. [[CrossRef](#)]
72. ElGamal, R.; Kishk, S.; Al-Rejaie, S.; ElMasry, G. Incorporation of a solar tracking system for enhancing the performance of solar air heaters in drying apple slices. *Renew. Energy* **2021**, *167*, 676–684. [[CrossRef](#)]
73. Kabeel, A.; Khalil, A.; Shalaby, S.; Zayed, M. Experimental investigation of thermal performance of flat and v-corrugated plate solar air heaters with and without PCM as thermal energy storage. *Energy Convers. Manag.* **2016**, *113*, 264–272. [[CrossRef](#)]
74. El Khadraoui, A.; Bouadila, S.; Kooli, S.; Farhat, A.; Guizani, A. Thermal behavior of indirect solar dryer: Nocturnal usage of solar air collector with PCM. *J. Clean. Prod.* **2017**, *148*, 37–48. [[CrossRef](#)]
75. Salih, S.M.; Jalil, J.M.; Najim, S.E. Experimental and numerical analysis of double-pass solar air heater utilizing multiple capsules PCM. *Renew. Energy* **2019**, *143*, 1053–1066. [[CrossRef](#)]
76. Abuşka, M.; Şevik, S.; Kayapınar, A. A comparative investigation of the effect of honeycomb core on the latent heat storage with PCM in solar air heater. *Appl. Therm. Eng.* **2019**, *148*, 684–693. [[CrossRef](#)]
77. Raj, A.; Srinivas, M.; Jayaraj, S. A cost-effective method to improve the performance of solar air heaters using discrete macro-encapsulated PCM capsules for drying applications. *Appl. Therm. Eng.* **2019**, *146*, 910–920. [[CrossRef](#)]
78. SunilRaj, B.; Eswaramoorthy, M. Experimental study on hybrid natural circulation type solar air heater with paraffin wax based thermal storage. *Mater. Today Proc.* **2020**, *23*, 49–52. [[CrossRef](#)]
79. Ameri, M.; Sardari, R.; Farzan, H. Thermal performance of a V-Corrugated serpentine solar air heater with integrated PCM: A comparative experimental study. *Renew. Energy* **2021**, *171*, 391–400. [[CrossRef](#)]
80. Mahdi, J.M.; Mohammed, H.I.; Talebizadehsardari, P.; Ghalambaz, M.; Majidi, H.S.; Khan, A.; Yaici, W.; Giddings, D. Simultaneous and consecutive charging and discharging of a PCM-based domestic air heater with metal foam. *Appl. Therm. Eng.* **2021**, *197*, 117408. [[CrossRef](#)]
81. Madhulatha, G.; Kumar, M.M.J.; Sateesh, P. Optimization of tube arrangement and phase change material for enhanced performance of solar air heater- A numerical analysis. *J. Energy Storage* **2021**, *41*, 102876. [[CrossRef](#)]
82. Dinesh, S.; Saminathan, R.; Patil, M.M.; Baviskar, P.R.; Hadidi, H.; Vignesh, S.; Kumar, P.M. Investigating the single pass baffled solar air heater (SAH) with an organic PCM (OPCM). *Mater. Today Proc.* **2022**, *62*, 5245–5249. [[CrossRef](#)]
83. Abu-Hamdeh, N.H.; Alsulami, R.A.; Hatamleh, R.I. A case study in the field of building sustainability energy: Performance enhancement of solar air heater equipped with PCM: A trade-off between energy consumption and absorbed energy. *J. Build. Eng.* **2022**, *48*, 103903. [[CrossRef](#)]
84. Palacio, M.; Ramírez, C.; Carmona, M.; Cortés, C. Effect of phase-change materials in the performance of a solar air heater. *Sol. Energy* **2022**, *247*, 385–396. [[CrossRef](#)]
85. Chaatouf, D.; Ghiaus, A.-G.; Amraqui, S. Optimization of a solar air heater using a phase change material for drying applications. *J. Energy Storage* **2022**, *55*, 105513. [[CrossRef](#)]
86. Verma, G.; Singh, S.; Chander, S.; Dhiman, P. Numerical investigation on transient thermal performance predictions of phase change material embedded solar air heater. *J. Energy Storage* **2022**, *47*, 103619. [[CrossRef](#)]
87. Sharol, A.; Razak, A.; Majid, Z.; Azmi, M.; Tarmizi, M.; Ming, Y.; Zakaria, Z.; Harun, M.; Fazlizan, A.; Sopian, K. Effect of thermal energy storage material on the performance of double-pass solar air heater with cross-matrix absorber. *J. Energy Storage* **2022**, *51*, 104494. [[CrossRef](#)]
88. Luo, Q.; Li, B.; Wang, Z.; Su, S.; Xiao, H. A study of unidirectional spiral tube for air evacuation in a solar heater with phase-change material. *J. Build. Eng.* **2022**, *46*, 103659. [[CrossRef](#)]
89. Farzan, H.; Zaim, E.H.; Amiri, T. Performance investigation on a new solar air heater using phase change material/expanded metal mesh composite as heat storage unit: An experimental study. *J. Energy Storage* **2022**, *47*, 103602. [[CrossRef](#)]

90. Fan, Z.; Zhao, Y.; Shi, Y.; Liu, X.; Jiang, D. Thermal performance evaluation of a novel building wall for lightweight building containing phase change materials and interlayer ventilation: An experimental study. *Energy Build.* **2023**, *278*, 112677. [[CrossRef](#)]
91. He, Z.; Ma, H.; Lu, S.; Sun, Y. Research on the thermal performance of interlayer ventilated PCM component coupled with solar air collector. *Energy Build.* **2022**, *255*, 111698. [[CrossRef](#)]
92. Brahma, B.; Shukla, A.K.; Baruah, D.C. Design and performance analysis of solar air heater with phase change materials. *J. Energy Storage* **2023**, *61*, 106809. [[CrossRef](#)]
93. SunilRaj, B.; Eswaramoorthy, M. Performance study on forced convection mode V-trough solar air heater with thermal storage: An experimental approach. *Mater. Today Proc.* **2023**, *72*, 1664–1672. [[CrossRef](#)]
94. Bayrak, F.; Oztop, H.F.; Hepbasli, A. Energy and exergy analyses of porous baffles inserted solar air heaters for building applications. *Energy Build.* **2013**, *5*, 338–345. [[CrossRef](#)]
95. Zhai, X.Q.; Song, Z.P.; Wang, R.Z. A review for the applications of solar chimneys in buildings. *Renew. Sustain. Energy Rev.* **2011**, *15*, 3757–3767. [[CrossRef](#)]
96. Tariq, R.; Torres-Aguilar, C.E.; Xamán, J.; Zavala-Guillén, I.; Bassam, A.; Ricalde, L.J.; Carvente, O. Digital twin models for optimization and global projection of building-integrated solar chimney. *Build. Environ.* **2022**, *213*, 108807. [[CrossRef](#)]
97. Yongcai, L.; Shuli, L.; Jun, L. Effects of various parameters of a PCM on thermal performance of a solar chimney. *Appl. Therm. Eng.* **2017**, *127*, 1119–1131. [[CrossRef](#)]
98. Liu, B.; Wang, M.; Wang, Q.; Mao, S.; Rachid, B. Effect of the Position of the Phase Change Material (PCM Na₂CO₃·10H₂O) on the Solar Chimney Effect. *Energy Procedia* **2017**, *139*, 462–467. [[CrossRef](#)]
99. Thantong, P.; Khedari, J.; Chantawong, P. Investigation of thermal performance by applying a solar chimney with PCM towards the natural ventilation of model house under Climate of Thailand. *Mater. Today Proc.* **2018**, *5*, 14862–14867. [[CrossRef](#)]
100. Fadaei, N.; Kasaeian, A.; Akbarzadeh, A.; Hashemabadi, S.H. Experimental investigation of solar chimney with phase change material (PCM). *Renew. Energy* **2018**, *123*, 26–35. [[CrossRef](#)]
101. Dordelly, J.C.F.; El Mankibi, M.; Roccamena, L.; Remion, G.; Landa, J.A. Experimental analysis of a PCM integrated solar chimney under laboratory conditions. *Solar Energy* **2019**, *188*, 1332–1348. [[CrossRef](#)]
102. Tiji, M.E.; Eisapour, M.; Yousefzadeh, R.; Azadian, M.; Talebizadehsardari, P. A numerical study of a PCM-based passive solar chimney with a finned absorber. *J. Build. Eng.* **2020**, *32*, 101516. [[CrossRef](#)]
103. Chen, W. Analysis of heat transfer and flow in the solar chimney with the sieve-plate thermal storage beds packed with phase change capsules. *Renew. Energy* **2020**, *157*, 491–501. [[CrossRef](#)]
104. Ashouri, M.; Hakkaki-Fard, A. Improving the performance of the finned absorber inclined rooftop solar chimney combined with composite PCM and PV module. *Solar Energy* **2021**, *228*, 562–574. [[CrossRef](#)]
105. Nateghi, S.; Jahangir, M.H. Performance evaluation of solar chimneys in providing the thermal comfort range of the building using phase change materials. *Clean. Mater.* **2022**, *5*, 100120. [[CrossRef](#)]
106. Li, W.; Li, Z.; Xie, L.; Li, Y.; Long, T.; Huang, S.; Lu, J.; Wang, Z. Evaluation of the thermal performance of an inclined solar chimney integrated with a phase change material. *Energy Build.* **2022**, *270*, 112288. [[CrossRef](#)]
107. Long, T.; Li, W.; Lv, Y.; Li, Y.; Liu, S.; Lu, J.; Huang, S.; Zhang, Y. Benefits of integrating phase-change material with solar chimney and earth-to-air heat exchanger system for passive ventilation and cooling in summer. *J. Energy Storage* **2022**, *48*, 104037. [[CrossRef](#)]
108. Koonsrisuk, A.; Chitsomboon, T. A single dimensionless variable for solar chimney power plant modeling. *Solar Energy* **2009**, *83*, 2136–2143. [[CrossRef](#)]
109. Koonsrisuk, A.; Chitsomboon, T. Dynamic similarity in solar chimney modeling. *Solar Energy* **2007**, *81*, 1439–1446. [[CrossRef](#)]
110. Koonsrisuk, A.; Chitsomboon, T. Partial geometric similarity for solar chimney power plant modeling. *Solar Energy* **2009**, *83*, 1611–1618. [[CrossRef](#)]
111. Ukrainczyk, N.; Kurajica, S.; Šipušić, J. Thermophysical comparison of five commercial paraffin waxes as latent heat storage materials. *Chem. Biochem. Eng. Q.* **2010**, *24*, 129–137.
112. Pielichowska, K.; Pielichowski, K. Phase change materials for thermal energy storage. *Prog. Mater. Sci.* **2014**, *65*, 67–123. [[CrossRef](#)]

Disclaimer/Publisher’s Note: The statements, opinions and data contained in all publications are solely those of the individual author(s) and contributor(s) and not of MDPI and/or the editor(s). MDPI and/or the editor(s) disclaim responsibility for any injury to people or property resulting from any ideas, methods, instructions or products referred to in the content.